Facultade de Ciencias do Mar
Universidade de Vigo

Máster Interuniversitario de Oceanografía

Trabajo de Fin de Máster

Curso 2020-2021

Master Interuniversitario en Oceanografía

THE IMPACT OF CLIMATE CHANGE ON THE GEOGRAPHICAL DISTRIBUTION OF HABITAT-FORMING MACROALGAE IN GALICIAN COAST

Beatriz Gutiérrez Martín

Supervisors: Dr. Marisela Des Villanueva; Dr. Ramón Gómez Gesteira

Index

Abstract

Climate change is causing pronounced shifts in the geographical distributions of intertidal canopy-forming macroalgae, especially at their warm-edge. The Northwest Iberian Peninsula (NWIP) coast is a vulnerable area as it is located at the southern distribution boundary of many species. *Himanthalia elongata* (*L.*) *S.F. Gray* and *Bifurcaria bifurcata R. Ross* are considered representatives of cold and warm-temperate affinity species, respectively. Because of it, they are used in the present work as potentially sensitive indicators of environmental changes due to climate change, in particular ocean warming. The Delft3D-Flow model was implemented, calibrated and validated for the NWIP coast. Then, numerical simulations for historical (1999-2018) and future periods (2080-2099) under Representative Concentration Pathway (RCP) 8.5 scenario were performed in order to simulate sea surface temperature (SST) data from Corcubion Bay to Ortegal Cape. Thus, a mechanistic distribution model based on the thermal tolerance threshold of *H. elongata* and *B. bifurcata* and heat waves was used to determine the suitability of the thermal habitats for these species for both periods. Results suggest a strong decline of *H. elongata* population and potential local extinction in the Artabro Gulf and Corcubion Bay by the end of the century. However, some spots may remain as climatic refugia for *H. elongata* along the study area, especially in the northernmost region, due to the upwelling pattern. This could prevent the total extinction of this species, and other cold-temperate fucoids, along NWIP. On the other hand, *B. bifurcata* populations, and other warm-temperate algae, are expected to persist and even occupy the free space left by the contraction of the cold-temperate species.

Keywords

canopy-forming seaweeds; climatic refugia; downscaling; numerical modelling; RCP 8.5.

Resumen

El cambio climático está causando variaciones significativas en la distribución geográfica de las macroalgas intermareales formadoras de hábitat, especialmente en el borde cálido. La costa Noroeste de la Península Ibérica (NWIP por sus siglas en inglés) es una zona vulnerable por tratarse del borde sur de la distribución de muchas de estas especies. *Himanthalia elongata* (*L.*) *S.F. Gray* y *Bifurcaria bifurcata R. Ross* son consideradas especies representativas de aquellas con afinidad a temperaturas frías y cálidas, respectivamente. Debido a ello, fueron elegidas en el presente trabajo como potenciales indicadores de los cambios ambientales producidos por el cambio climático, en particular el calentamiento oceánico. El modelo Delft3D-Flow fue implementado, calibrado y validado para la costa NWIP. Posteriormente, se realizaron simulaciones numéricas para el periodo histórico (1999-2018) y futuro (2080-2099) bajo el escenario 8.5 de las trayectorias de concentración representativas (*Representative Concentration Pathway* en inglés, RCP 8.5) para simular la temperatura superficial del mar (*Sea Surface Temperature* en inglés, SST) desde la Bahía de Corcubión hasta Cabo Ortegal. A continuación, se usó un modelo mecanicista de distribución de especies basado en el umbral térmico de tolerancia de *H. elongata* y *B. bifurcata* y en las olas de calor, para determinar la idoneidad de los hábitats térmicos de estas especies en ambos periodos. Los resultados sugieren un fuerte declive de *H. elongata* y una potencial extinción local en el Golfo Ártabro y la Bahía de Corcubión a finales de siglo. Sin embargo, algunas zonas podrían mantenerse como refugios climáticos para *H. elongata* a lo largo de la zona de estudio, especialmente en la región más al norte, debido a los patrones de afloramiento. Esto podría prevenir la extinción total de esta especie, y de otras algas afines a temperaturas frías, a lo largo de la costa NWIP. Por otro lado, se espera que *B. bifurcata*, y otras algas afines a temperaturas cálidas, persistan e incluso lleguen a ocupar el espacio vacío dejado por la contracción de las especies afines a temperaturas frías.

Palabras clave

algas formadoras de hábitat; RCP 8.5; refugio climático; regionalización; modelado numérico.

Resumo

O cambio climático está a causar variacións significativas na distribución xeográfica das macroalgas intermareais formadoras de hábitat, especialmente no borde cálido. A costa Noroeste da Península Ibérica (NWIP polas siglas en inglés) é unha zona vulnerable ó tratarse do borde sur da distribución de moitas destas especies. *Himanthalia elongata* (*L.*) *S.F. Gray* e *Bifurcaria bifurcata R. Ross* son consideradas especies representativas daquelas afíns a temperaturas frías e cálidas respectivamente. Por iso, escolléronse no presente traballo como potenciais indicadores dos cambios ambientais producidos polo cambio climático, en particular polo quecemento oceánico. O modelo Delft3D-Flow implementouse, calibrouse e validouse para a costa NWIP. Despois, fixéronse simulacións numéricas para o período histórico (1999-2018) e futuro (2080-2099) baixo o escenario 8.5 das traxectorias de concentración representativa (*Representative Concentration Pathway* no inglés, RCP 8.5) para simular a temperatura superficial do mar (*Sea Surface Temperature* no inglés, SST) dende a Baia de Corcubión ata Cabo Ortegal. A continuación, usouse un modelo mecanicista de distribución de especies baseado no límite térmico de tolerancia de *H. elongata* e *B. bifurcata* e nas vagas de calor, para determinar a idoneidade dos hábitats térmicos destas especies en ambos períodos. Os resultados suxiren un forte declive de *H. elongata* e unha potencial extinción local no Golfo Ártabro e na Baía de Corcubión a finais de século. Con todo, algunhas zonas poderían mantérense coma refuxios climáticos para *H. elongata* ao longo da zona de estudio, especialmente na rexión máis ao norte, debido aos patróns de afloramento. Isto podería precaver a extinción total desta especie, e doutras algas afíns a temperaturas frías, ao longo da costa NWIP. Por outra banda, esperase que *B. bifurcata*, e outras algas afíns a temperaturas cálidas, persistan e incluso cheguen a ocupar o espazo baleiro deixado pola contracción das especies afíns a temperaturas frías.

Palabras clave

algas formadoras de hábitat; RCP8.5; refuxio climático; rexionalización; modelado numérico.

1. Introduction

One of the most evident signs of climate change is global warming, and over the last decades, it has significantly impacted terrestrial and marine ecosystems worldwide. Recent shifts in the geographic ranges of marine and terrestrial species have been linked to the increase in air temperature and ocean warming (Walther et al., 2002; Gaston, 2003; Parmesan et al., 2005; Sagarin et al., 2006; Thomas et al., 2006; Lima et al., 2007; Beaugrand et al., 2008; Gaston, 2009). Species show range expansions poleward and range contractions at the low-latitude limit (warn edge) of their distributions, where temperatures are no longer tolerable (Pecl et al., 2017). These contractions may end up in local extinctions reducing global biodiversity (Wiens, 2016). Range-edge populations are of vital importance, as they primarily determine the sensibility of species to range shifts, especially under future climates where extreme climatic events are predicted to increase (Rehm et al., 2015). Peripheral populations can inhabit favorable local habitats at their limit range, known as climate refugia, which are safe but more vulnerable to climate change due to their location at the warm edge (Ashcroft, 2010). Global warming has increased over the last years and is predicted to continue this trend over the next century (IPCC, 2001; Burrows et al., 2011; Merzouk and Johnson, 2011). Therefore, climate refugia may mitigate the retreat of species at their range limit predicted under climate change (Duarte and Viejo, 2018).

In the marine environment, the major consequence of climate change is the increase in water temperature (Merzouk and Johnson, 2011); in particular, at range limits of species, distribution populations are smaller and thermal conditions are closer to their tolerance limit. However, there are other consequences, such as acidification and oxygen loss (Bindoff et al., 2019), sea-level rise, changes in circulation patterns and intensification of extreme events (both in frequency and severity, i.e. heat waves) that will impact marine organisms. Since the upwelling-affected coastal areas have a lower tendency to warming than in the open shore and adjacent coastal areas (Alvarez et al., 2009; Santos et al., 2011, 2012; Varela et al., 2018; Seabra et al., 2019), they may represent climate refugia against ocean warming for many species, especially to cold-affinities species in their southern distribution limits (Lourenco et al., 2016). On the other hand, as Bakun (1990)

hypothesized, and several authors predicted later on for different upwelling systems (Casabella et al., 2014; Sydeman et al., 2014; Varela et al., 2015; Wang et al., 2015; Sousa et al., 2017) upwelling-favorable winds may be intensified due to an increase in the thermal gradient between land and ocean. However, ocean warming may increase the stratification of the ocean upper layers, leading to a less effective upwelling despite the intensification of upwelling-favorable winds (Sousa et al., 2020). Therefore, upwelling coastal patterns will mainly depend on the intensification of upwelling-favorable winds and the increase of thermal stratification, which will become more severe under climate change and may counteract these winds (Sousa et al., 2020). Despite this, the upwelling areas may continue to act as a climatic refugia in future since the water temperature in these areas would continue to be lower than that of the surrounding ocean (Des et al., 2020b).

Rocky shore ecosystems of temperate coasts, typically dominated by canopy-forming seaweeds, are considered one of the most productive and ecologically important areas, especially those affected by upwelling (Steneck et al., 2002; Smale et al., 2013; Bennett et al., 2015). Canopy-forming macroalgae are intertidal foundation species that often live close to their physiological tolerance thresholds (Helmuth et al., 2006; Martínez et al., 2012). Therefore they are considered early indicators of the impact of climate change (Jueterbock et al., 2013). Furthermore, these foundation species are ecologically important because they are ecosystem engineers, providing habitat, shelter and food for many associated sessile animals and fish communities (Jones et al., 1997; Teagle et al., 2017; Pessarrodona et al., 2019). Therefore, shifts in their geographical distribution may trigger changes in the whole coastal ecosystem (Schiel, 2006). Several authors have documented strong declines of canopy-forming seaweeds populations in the warm edge of their distribution (Nicastro et al., 2013; Smale and Wernberg, 2013; Fernández, 2016), mainly attributed to the increase of sea surface temperature (SST) along with more frequent and intense climate-driven extreme events (Duarte et al., 2013; Smale and Wernberg, 2013; Wernberg et al., 2013, 2016; Krumhansl et al., 2016). In particular, these rage contractions may affect more significantly to cold-affinity species due to their higher sensitivity to rises in sea surface temperature (Luning et al., 1990). Globally, as the Intergovernmental Panel on Climate Change (IPCC, 2019) states, the level of risk for kelp forests ecosystems is projected to increase significantly over the 21st century, with more than 50% richness loss

in some areas (Wilson et al., 2019). An increasing number of studies have shown upwelling-coastal areas may act as contemporary refugia from ocean warming to these vulnerable populations (Ashcroft, 2010; Keppel et al., 2012; Lourenço et al., 2016; Duarte and Viejo, 2018; Casado-Amezúa et al., 2019). For all of this, contemporary refugia play a key role in the conservation of edge populations threatened by climate change (Keppel et al., 2012) and at risk of local extinction, preserving by this way global biodiversity (Lourenço et al., 2016).

The Northwest Iberian Peninsula (NWIP), located in the northern limit of the Eastern North Atlantic Upwelling system, is the thermal southern range boundary for several intertidal canopy-forming macroalgae and kelps. Several authors have documented climate-driven shifts in the distributions of these species in this area (Martínez et al., 2012; Duarte et al., 2013; Casado-Amezúa et al., 2019; Des et al., 2020b), showing different responses among species, with a drastic retraction of cold-temperate species. Cold-temperate macroalgae are abundant at the NWIP but absent from the eastern Cantabria Sea (northern Spain) and southern Portugal, where warm-temperate species are mostly found (Luning et al., 1990). This distribution pattern has been related to upwelling events present in the NWIP and warmer conditions towards the eastern part of the Cantabria Sea (Gómez-Gesteira et al., 2008; Michel et al., 2009).

The two intertidal foundation species *Himanthalia elongata (L.) S.F. Gray* and *Bifurcaria bifurcata R. Ross* were chosen in the present work due to their cold-temperate and warm-temperate affinities, respectively. The distribution of these species is significantly correlated with the increase of seawater temperature (Martínez et al., 2012; Duarte et al., 2013), being potentially sensitive indicators of variations due to climate change (Martínez et al., 2015). A significant range contraction of *H. elongata* distribution has been observed in recent years, virtually vanishing in Northern Spain (Duarte et al., 2013), whereas *B. bifurcata* has increased in abundance along the north and northwest coast of the Iberian Peninsula (Ramos et al., 2020). The observed decline of *H. elongata* in contrast with the expansion of *B. bifurcata* may reflect a higher resistance of *B. bifurcata* to increasing SST due to a higher physiological tolerance threshold (24.7°C) in comparison with *H. elongata's* limit (18°C) (Martínez et al., 2012). Future projections predict a local

extinction of *H. elongata* in the Cantabrian Sea (northern Spain) at a faster rate than in the NWIP and an increase in abundance of *B. bifurcata* in both regions under future warming scenarios (Martínez et al., 2012). On the other hand, Des et al. (2020b) have determined that the Rías Baixas acts as contemporary refugia for *H. elongata* and other cold-temperate seaweeds. However, they predict that it may become extinct in this area by the end of the century, while *B.bifurcata* may persist and likely increase in abundance, taking advantage of the decline of *H. elongata* and occupying their potential empty localities.

The Galician coast (Figure 1), northwest corner of the Iberian Peninsula, is considered one of the most economically and ecologically important coastal areas due to its location on the northern limit of the Eastern North Atlantic Upwelling system. In this area, the upwelled cold deep water pumps a high concentration of nutrients to the surface (Prego et al., 1999), increasing primary production. The study area, covering from Corcubion Bay to Ortegal Cape (Figure 1), is affected by upwelling events, mainly during the summer. These events occur in the far eastern areas of the Artabro Gulf (Prego and Varela, 1998) and to the north of Finisterre Cape (Prego and Bao, 1997), remaining the rias of Ferrol, Ares-Betanzos and A Coruña isolated from upwelling due to the topographic features of the Artabro Gulf (Prego and Varela, 1998). Furthermore, upwelling to the north of Finisterre Cape is discontinuous and keeps distant from the coast (Prego and Bao, 1997). Alvarez et al. (2010) indicated that the upwelling events observed in the study area are less common and less intense than along the remaining NWIP coast. Sousa et al. (2020) observed that in most of the NWIP coast, the upwelling' effectiveness could be reduced; however, their projections show that, in the study area, it may maintain or even intensify in some areas. Therefore, the study area could continue to act as a climatic refugia for cold-temperate species, preventing their total extinction off NWIP coast. This work is the first known research about the impact of climate change on the geographical distribution of canopy-habitat seaweeds in the study area and the role of the local ocean circulation that may help to prevent their local extinction. Nowadays, numerical models are considered as one of the best tools to perform this task. They are capable of reproducing reality accurately and make projections under different scenarios of climate change in the future.

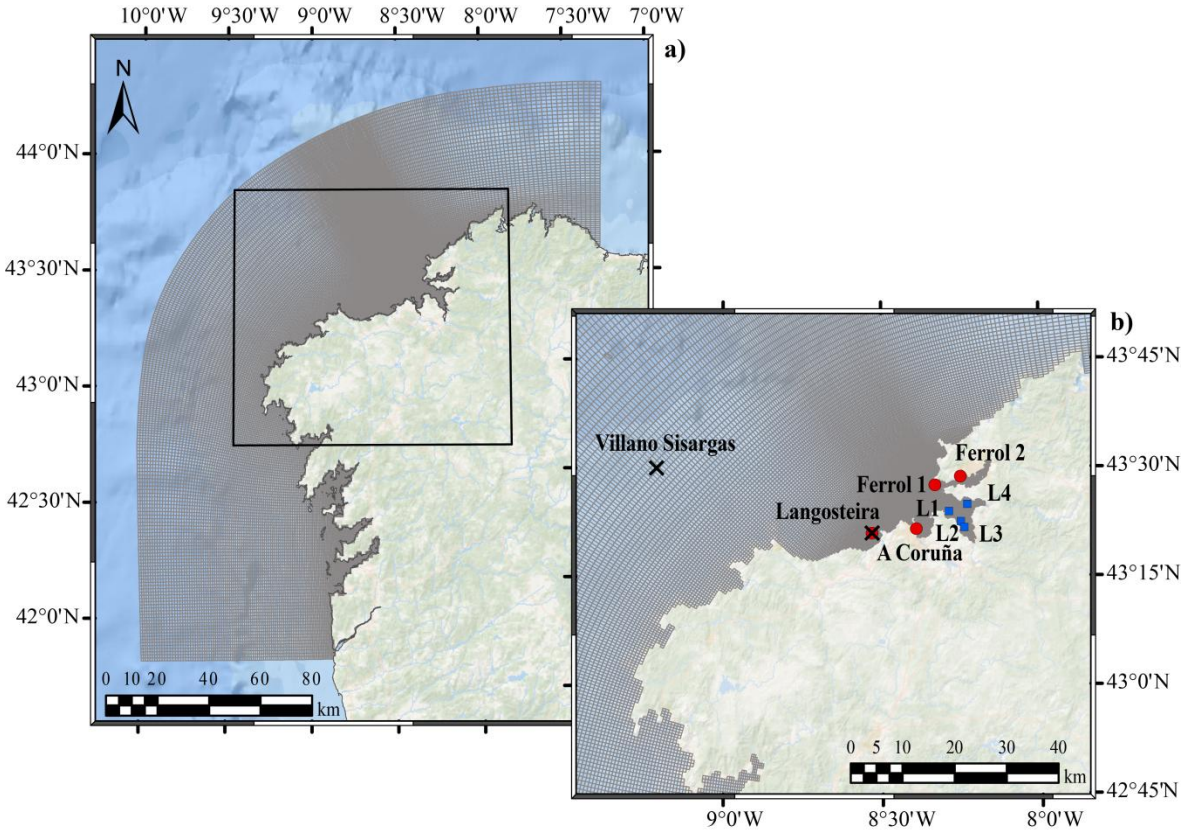

Figure 1. Location of the study area (box) along the northwestern coast of the Iberian Peninsula (a). The computational grid is shown in grey. A close-up view of the study area (b) showing the position of *Puertos del Estado* tidal gauges (red circles), Villano Sisargas and Langosteira buoys (cross) and *INTECMAR* sampling stations (blue square).

Coupled Model Intercomparison Project Phase 5 (CMIP5) framework makes available to the scientist community the outputs of several Global Circulation Models (GCMs). However, these models do not have the spatial resolution necessary to capture the hydrodynamic processes of the study area. For that reason, it is necessary to perform a downscaling of the GCMs. In this work, the Delft-3D hydrodynamic model was chosen to perform the downscaling, being necessary to calibrate and validate it for the study area. The capability of numerical model Delft3D-Flow to reproduce the hydrodynamic conditions of coastal and estuarine areas was previously assessed by several authors (Iglesias et al., 2008; Carballo et al., 2009a, 2009b; Iglesias and Carballo, 2009, 2010a, 2010b; Des et al., 2019, 2020a, 2020b).

Due to the nature of the GCMs outputs (monthly climatological data), the validation and calibration process cannot be done by comparing the model's output at a specific

moment with the corresponding field data, being necessary to compare climatologies. For this reason, firstly, Delft3D-Flow should be implemented under realistic conditions (Exp#1), validating and calibrating the model by comparing outputs with field data. And then, Delft3D-Flow should be implemented under climatological conditions (using the GCMs as input, Exp#2). Finally, Exp#1 outputs could be used to calibrate and validate Exp#2. GCMs offer outputs for historical and future periods under the Representative Concentration Pathway (RCP) scenarios proposed by the IPCC (2014), including the business-as-usual climate change scenario (RCP 8.5), representing the most pessimistic conditions but also the most likely according to the greenhouse gas emissions evolution (Brown and Caldeira, 2017). Thus, once the model is implemented for an area, it can be used to perform the downscaling of all these data.

1.1. Hypothesis and objectives

The study hypothesis is that some areas of the Galician coast may remain as climatic refugia for cold-temperate macroalgae species (represented by *H. elongata*) by the end of the century, including the business-as-usual climate change scenario, due to the upwelling pattern. In addition, free locations where these species could become extinct may be occupied by warm-temperate macroalgae species (represented by *B. bifurcata*).

The objectives of the study are:

- To implement, calibrate and validate the Delft3D hydrodynamic model for the area covering from Corcubion Bay to Ortegal Cape.
- To perform a downscaling of GCMs for July-August for historical (1999-2018) and future (2080-2099) periods under the RCP8.5.
- To analyze whether the study area may act as potential climatic refugia for cold-temperate foundation macroalgae by considering *H. elongata* as representative species.
- To analyze the potential expansion of warm-temperate foundation macroalgae in the study area, by considering *B. bifurcata* as representative species, by the end of the century.
- To detect areas where both types of species could coexist and potential local extinctions.

2. Data and Methods

2.1. Data

Data of different nature was required for the model as input data to accurately simulate the hydrodynamics of the study area, such as hydrographic and atmospheric conditions, freshwater discharges, tidal constituents and bathymetry. Forcing the model with realistic data requires different nature of data than forcing it with climatological data. For that reason, the same input variable may come from different sources depending on the objective of the experiment. Furthermore, during the validation and calibration of the model, data from additional data sources were required to be compared with simulations outputs in order to assess the model accuracy. This section will cover all these types of data sources and their main features. Each of them provides the most adequate spatial and temporal resolution in order to achieve the best simulations.

2.1.1. Hydrographic data

Hourly near-surface (3 m depth) transport conditions at Estaca de Bares (water temperature and salinity), Villano Sisargas (water temperature and salinity) and Langosteira (water temperature) buoys (Figure 1) were retrieved from **Puertos del Estado** (http://www.puertos.es) for the period July-August 2015. These data were used to assess the model capability (run under realistic conditions) to reproduce transport conditions.

Vertical profiles of salinity and water temperature were provided by the Instituto Tecnolóxico Para O Control Do Medio Mariño De Galicia (**Intecmar,** http://www.intecmar.gal/) for the period July-August 2015. Data were collected in weekly sea surveys with a SBE25 CTD from the following sampling stations: L1, L2, L3 and L4 (Figure 1). These data were used to evaluate the accuracy of the model (run under realistic conditions) in reproducing thermohaline variables.

High-resolution SST data, provided by **MODIS-Aqua and MODIS-Terra** satellite sensors for July-August 2015, were retrieved from the NASA Ocean Color website (http://oceancolor.gsfc.nasa.gov). Because of the complexity to distinguish between SST and land surface temperature, a mask of 3 × 3 was applied following the shoreline (Mendes

et al., 2014). A filter has also been used to eliminate the data associated with cloud cover (Mendes et al., 2014). Satellite SST data were used to test the model's capability (run under realistic conditions) in reproducing the SST.

Transport conditions, daily average 3D salinity and water temperature data were retrieved from the **Atlantic-Iberian Biscay Irish-Ocean Physics Reanalysis** (ibi_multiyear_phy_005_002), with a horizontal resolution of 1/12° and 50 vertical levels. Data were obtained through the Copernicus Marine Service website (http://marine.copernicus.eu) for July-August 2008-2019. Data were imposed on the model as ocean-open boundary conditions in realistic simulations.

Monthly seawater salinity and temperature were obtained from the Hadley Centre Global Environment Model - version 2 Earth System (MOHC-HadGEM2-Es) Global Circulation Model (GCM). This model is run within the framework of **Coupled Model Intercomparison Project Phase 5** (**CMIP5**, https://www.wcrp-climate.org/wgcm-cmip/wgcm-cmip5). Climatological data were downloaded for the historical (July-August 1999-2018) and the future (July-August 2080-2099) periods under historical and Representative Concentration Pathway (RCP) 8.5 greenhouse gas emissions scenario (https://esgf-node.ipsl.upmc.fr/projects/esgf-ipsl/). The MOHC-HadGEM2-Es model has an ocean resolution of 1° (increasing to 1/3° at the equator) and 40 vertical levels, being considered the best model in reproducing historical data under climatological conditions for the study area (Sousa et al., 2020). These data were imposed on the model as ocean-open boundary conditions in climatological experiments.

2.1.2. Tide Constituents

Water level data measured every ten minutes at A Coruña 2, Ferrol 1, Ferrol 2 and Langosteira **Puertos del Estado's gauge stations** were retrieved from *Puertos del Estado* web portal (http://www.puertos.es/en-us) for July-August 2015. These data were used to compare against model simulations in order to reproduce accurately tidal conditions.

Thirteen tidal harmonic constituents (M_2, S_2, N_2, K_2, K_1, O_1, P_1, Q_1, MF, MM, M_4, MS_4 and MN_4) were obtained from the **TPXO 7.2 TOPEX/Poseidon Altimetry model** (http://volkov.oce.orst.edu/tides/global.html) with a horizontal resolution of ~ 25 km

(MacMillan et al., 2004). These data were imposed on the model as ocean-open boundary conditions, prescribed as astronomic forcing.

2.1.3. Atmospheric Data

Hourly meteorological data (air temperature, net solar radiation, relative humidity, sea level pressure and u and v wind components) with a spatial resolution of 4km was retrieved from the Weather Research and Forecasting Model (WRF) run by the Galician regional meteorological agency (**MeteoGalicia,** www.meteogalicia.gal**)** for July-August 2009-2018. These data were imposed on the model as surface-open boundary conditions in realistic simulations.

Atmospheric climatological data (3 hours temporal resolution surface air temperature, net solar radiation, relative humidity, sea level pressure, and 6 hours zonal and meridional wind components) were provided by the **MOHC-HadGEM2-Es-RCA4** Regional Climate Model **(RCM)**. This regional model is run within the framework of the Coordinated Regional Climate Downscaling Experiment project (**CORDEX,** https://www.cordex.org) and has a horizontal resolution of 0.11°. MOHC-HadGEM2-Es-RCA4 is the downscaling of the MOHC-HadGEM2-Es GCM with the RCA4 model, and it is considered the most accurate climate model in reproducing historical data in the area of study (Sousa et al., 2020). Data were downloaded for the historical (July-August 1999-2018) and future (July-August 2080-2099) periods and were imposed on the model as surface-open boundary conditions in climatological experiments.

2.1.4. Bathymetry

The bathymetry of the area of study defines the bottom topography. It was obtained from the General Bathymetry Chart of the Oceans (GEBCO, https://www.gebco.net), with a spatial resolution of 30 arc-second intervals.

2.1.5. River Discharge Data

Daily freshwater discharges for the main rivers of the modelled area (Anllons, Belelle, Eume, Mandeo, Mero, Xallas, Xubia, Tambre, Ulla, Umia, Lerez and Verdugo) were

downloaded from **MeteoGalicia website** (www.meteogalicia.gal). These measured river discharges were retrieved for the historical period (July-August 2009-2018).

Daily modelled river discharges for the main rivers were downloaded from the **Hype Web portal** (https://hypeweb.smhi.se/) for all available period (1981-2010). These data were imposed on the model in experiments covering 1999-2008, since no field data are available for this period. Moreover, these data were used to perform a climatology of the discharge of each of the rivers. These data were used as input on future projection experiments by applying a reduction of 25 % in river discharge, following projections for the modelled area by the end of the century under a RCP8.5 greenhouse gas emission scenario (https://hypeweb.smhi.se/explore-water/climate-change-data/europe-climate-change/). River discharges were imposed on the model as fluvial open boundary conditions.

2.2.Hydrodynamic model (Delft3D-Flow)

The numerical model Delft3D solves the horizontal equations of motion, the continuity equation and the transport equation for conservative constituents under the shallow water assumption. The numerical method of Delft3D-Flow is based on finite differences. Further information about Delft3D model could be found in Lesser et al. (2004) and Grunnet et al. (2004). The numerical simulations of this study were performed using the **Flow module** (Delft3D-Flow research version 4.04.01), which simulates the hydrodynamic flow and calculates heat and salinity transport along the computational grid resulting from tidal and meteorological forcing, including the effect of a non-uniform distribution of temperature and salinity. For that purpose, the model requires water level, salinity, water temperature, river discharge and meteorological conditions. Delft3D model was designed for numerical modelling of coastal, river and estuarine areas using 2D or 3D approaches. The 3D approach was used in this work because it is most appropriate for coastal and estuarine areas where there is a significant variation of the horizontal flow field in the vertical direction (Deltares, 2014), as the study area shows.

2.2.1. Main features

The modelled area was covered by a well-structured, orthogonal irregular curvilinear **grid**. A spherical coordinate system was chosen to allow the bathymetry to follow the Earth´s curvature. The grid dimensions are defined by 364 grid cells in the M-direction and 213 grid cells in the N-direction, with a total of 34518 grid elements. The covered area ranges from 10.08° W to 7.29° W and from 41.82° N to 44.30° N (Figure 1). The computational grid used a **unique-domain approach** with a horizontal resolution of 124 m × 82 in the study area, increasing gradually to 2682 m x 1586 m at the ocean open boundary (Table 1).

The complex hydrodynamic of the study area requires a modelled area covering a larger region than the concrete study area to properly solve the hydrodynamic processes in the study area and avoid the disturbances associated with open boundaries.

Table 1. Main features of the computational grid under the area of study.

Feature	Specification
Domain	10.08° W to 7.29° W 41.82° N to 44.30° N
Horizontal resolution	From 2682 x 1586 m on the ocean open boundary to 124 x 82 m in the Galician rias of Ferrol, A Coruña and Ares-Betanzos.
Vertical resolution	16 sigma layers, with top layers refined
Oceanic boundary forcing – Tidal forces	Water level, 13 harmonic constituents, as astronomical forcing
Oceanic boundary forcing – Transport conditions	Salinity and water temperature, both specified per layer

The grid cells are defined with the water level and density properties calculated in the centre of the cell and the velocity components (u, v) located perpendicular to the cell. In the vertical direction, sixteen **vertical sigma layers** were used (Figure 2). Surface layers were refined in order to reproduce the ocean-atmospheric interaction accurately. A sigma layer approach means that the number of layers is constant along the computational grid, and

each layer represents a percentage of the depth in each cell of the domain. The percentage of depth assigned for each layer in this study is, 1st layer 1%, 2nd layer 1%, 3rd layer 3%, 4th layer 4%, 5th layer 5%, 6th layer 6%, from 7th to 16th layers 8% each.

Along the numerical grid, four-set **observation points** were defined at the same position as buoys and gauge stations from *Puertos del Estado* and sample stations of *Intecmar*. These observations points were used to evaluate the model accuracy in reproducing flow and transport conditions for the historical period under realistic conditions. Grid points excluded from being flooded during simulation (such as islands) were defined as **dry points**, and therefore flow and transport conditions were not calculated in those cells. Finally, **thin damps** were used to represent small obstacles in the grid, such as break-waters, that block the flow between two adjacent grid cells but without influence on the water volume of the model.

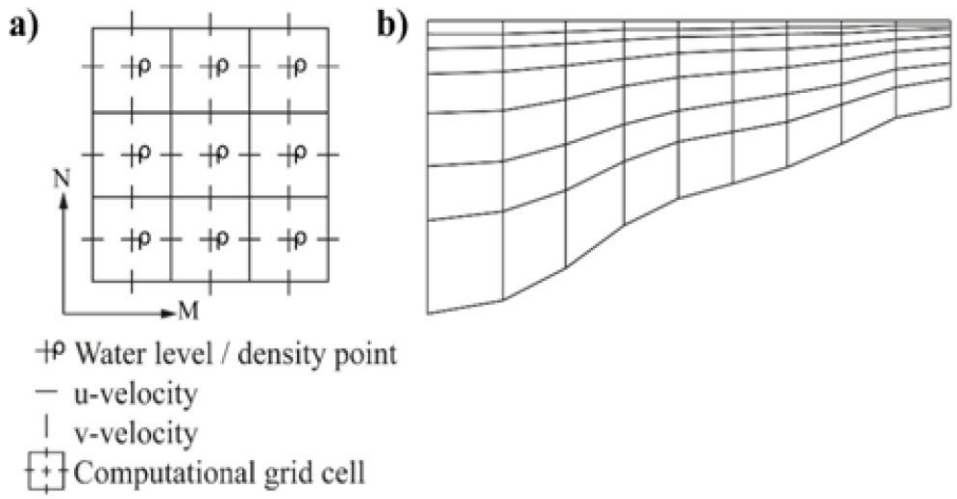

Figure 2. Horizontal a) and vertical b) grid of Delft3D-Flow. From Des (2020).

2.2.2. Input Data

Initial conditions are the initial values of water level, flow velocity components, water temperature and salinity provided to each cell of the computational grid at the start of the numerical simulations.

Boundary conditions provide the influence of the non-modelled area surrounding the computational grid. The **ocean-open boundary** was formed by 104 sections, fed with

transport conditions (water temperature and salinity) specified per layer and water level (defined as **astronomic forcing**). The **surface-open boundary** was fed with atmospheric data varying spatially. Freshwater discharges were imposed on the model as **fluvial-open boundary conditions**. The **close boundaries** were defined by the coastline and the bathymetry.

2.2.3. *Model implementation*

Two numerical experiments were defined in this work, Exp#1 and Exp#2, to simulate the hydrodynamic processes of the study area under realistic and climatological conditions, respectively. These experiments were based on the procedure follows by Des et al. (2019, 2020a) in the Rías Baixas. In this work, Exp#1 and Exp#2 shared the domain (Table 1), bathymetry and tidal harmonic constituents. However, the initial and boundary conditions came from different data sources, depending on the experiment. The diagram flow shown in Figure 3 represents the different data sources that provide initial and boundary conditions to the model, in both Exp#1 and Exp#2, as well as the model outputs and their connection with the mechanistic distribution model.

The first experiment (**Exp#**1) was forced with **realistic data** and ran for July and August from 2009 to 2018 (10 runs). For these simulations, transport conditions (water temperature and salinity) were obtained from Atlantic-Iberian Biscay Irish-Ocean Physics Reanalysis (Section 2.1.1), atmospheric variables (Section 2.1.3) and river discharges (Section 2.1.5) from the MeteoGalicia database.

The second experiment (**Exp#2)** was forced with **climatological data**. Firstly, the simulations covering July-August 2009-2018 were run and used to calibrate and validate this experiment by comparing against Exp#1. Once the Exp#2 was validated, it was extended, covering July and August from 1999 to 2018 under historical conditions and from 2080 to 2099 under the RCP 8.5 scenario (a total of 40 runs). The inputs of this experiment come from the MOHC-HadGEM2-Es GCM (Section 2.1.1) as transport conditions, the MOHC-HadGEM2-Es-RCA4 RCM (Section 2.1.3) as atmospheric variables and the Hype Web Portal (Section 2.1.5) as river discharges.

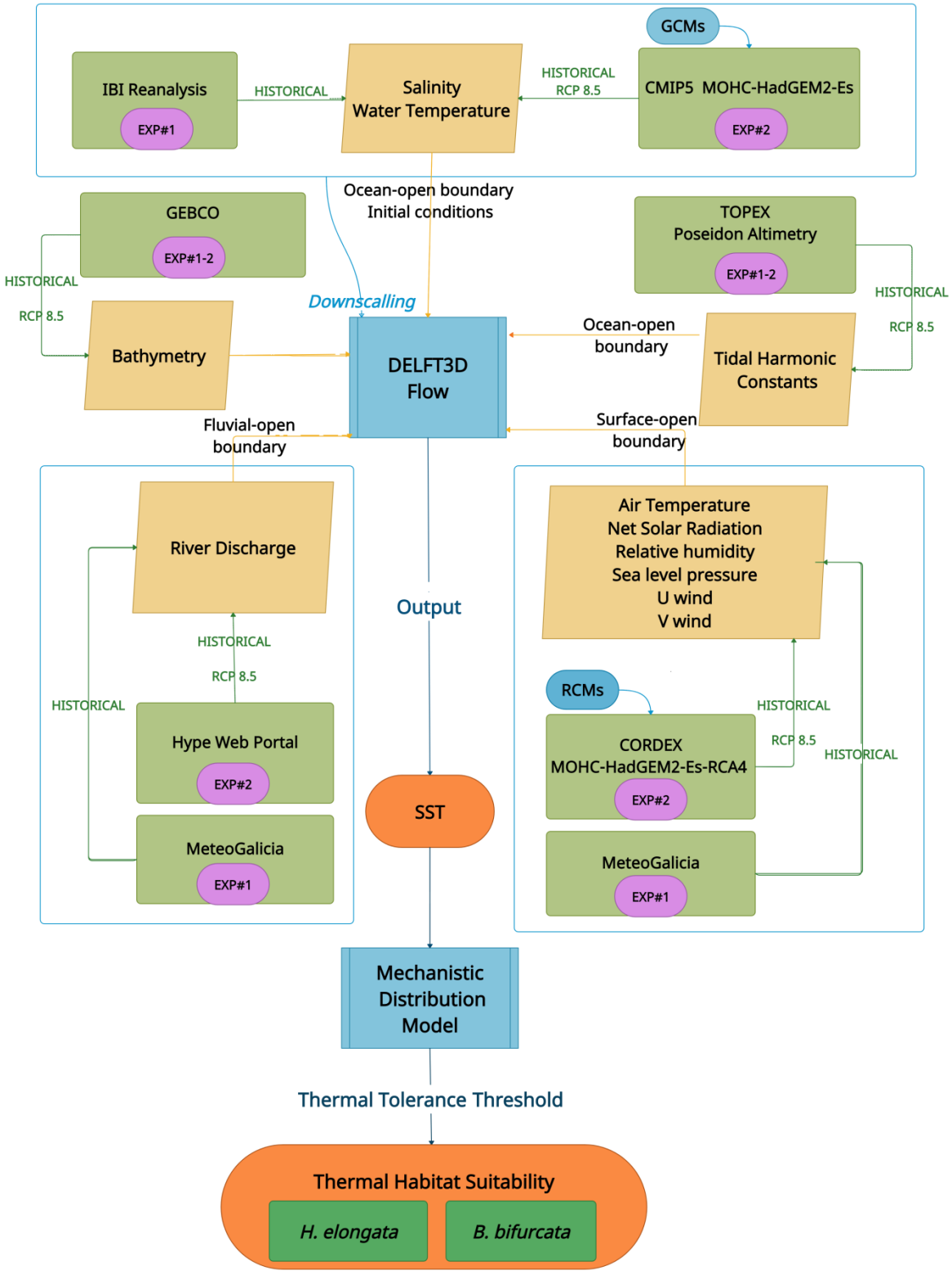

Figure 3. Initial and boundary conditions of the experiments Exp#1 and Exp#2 and the connection between the Delft3D-Flow module and the Mechanistic Distribution Model.

2.2.4. Model validation and calibration

The validation and calibration process is required to accurately assess the model's skill to reproduce the hydrodynamic of the study area. This process starts setting up the **parameterization of the model**, which includes the physical parameters (bottom roughness coefficient, viscosity and diffusivity) and the heat flux model used for the domain. Firstly, these parameters were determined following previous studies on similar regions (Sousa et al., 2018, 2020; Des et al., 2019, 2020a). Then, the model was executed, and the results were cross-checked against historical data, which could be observed data (Exp#1) or computed data from other validated simulations (Exp#2). This process was repeated, modifying the model's calibration parameters until the accuracy of the model was good enough and the parameterization can be considered valid.

The **model validation and calibration procedures** followed in this work are similar to those proposed by Des et al. (2019, 2020a). The validation and calibration of the model forced with realistic conditions (Exp#1) was performed by cross-checking results from simulations against observed data for July-August 2015 (Figure 4). The cross-checking method was conducted by comparing computed sea surface elevation (SSE), near-surface seawater salinity and temperature, and salinity and water temperature vertical profiles.

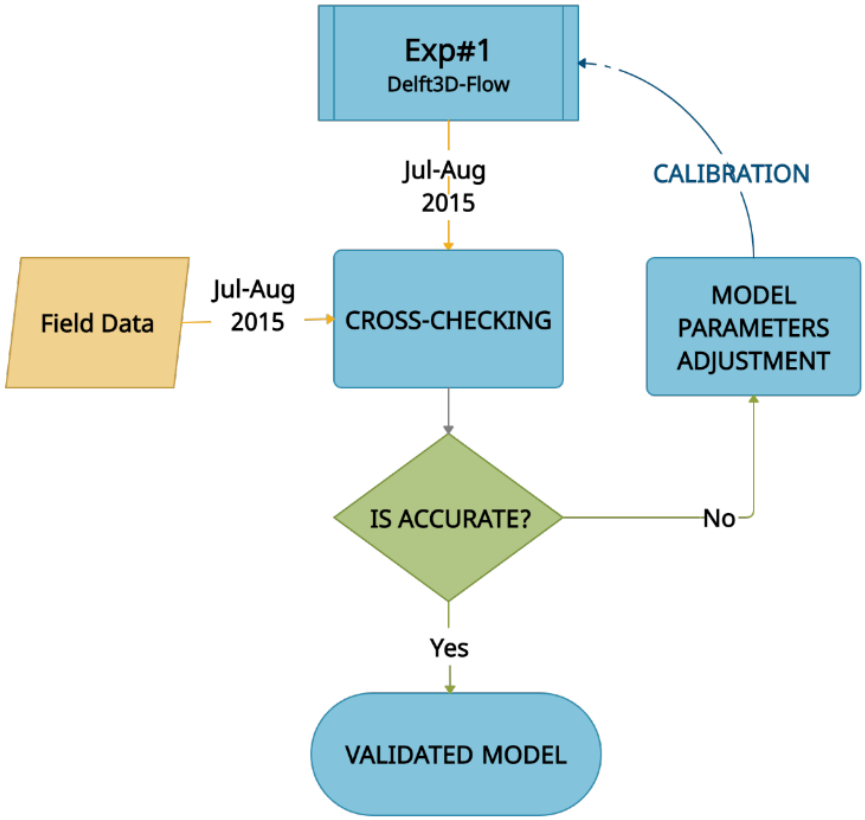

Figure 4. Validation and calibration method of the model forced with realistic conditions (Exp#1).

The statistical procedure adopted during this work to evaluate the model accuracy is based on Dias et al. (2009) for the Ría Formosa (Portugal) and Des et al. (2019, 2020b) for the Rías Baixas. Data was retrieved, prepared and compared using custom matlab® components.

Water level and main tidal harmonic constants (S2, M2, O1 and K1) were compared using the T_TIDE matlab® package Pawlowicz et al. (2002).

The statistical analysis used to validate the accuracy of the model was conducted using the root mean square error (RMSE), predictive skill (Skill), standard deviation and bias indicators.

RMSE was calculated as:

$$RMSE = \left\{ \frac{1}{N} \sum_{i=1}^{N} |X_{mod}(t_i) - X_{obs}(t_i)|^2 \right\}^{1/2}$$

where N is the number of samples used in the measured data and the number of time steps used for the model, and $X_{obs}(t_i)$ and $X_{mod}(t_i)$ are the values retrieved from measured and model predictions, respectively.

The predictive skill is based on the quantitative agreement between measured data and computed results (Warner et al., 2005). It was calculated as:

$$Skill = 1 - \frac{\sum_{i=1}^{N} |X_{mod}(t_i) - X_{obs}(t_i)|^2}{\sum_{i=1}^{N} \left(\left| X_{mod}(t_i) - \overline{X_{obs}(t_i)} \right| + \left| X_{obs}(t_i) - \overline{X_{obs}(t_i)} \right| \right)^2}$$

where the horizontal bar represents mean values, and $X_{obs}(t_i)$ and $X_{mod}(t_i)$ are the values retrieved from measured and model predictions, respectively. A skill value of 1 indicates a perfect agreement between observations and the model, values higher than 0.95 represent an excellent agreement and a value of zero means complete disagreement (Dias et al., 2009).

The standard deviation was calculated as:

$$\sigma(X) = \sqrt{\frac{\sum_{i=1}^{N} \left(\left| X_{mod}(t_i) - \overline{X_{mod}(t_i)} \right| + \left| X_{obs}(t_i) - \overline{X_{obs}(t_i)} \right| \right)^2}{N - 1}}$$

where N is the number of samples and $X_{mod}(t_i)$ and $X_{obs}(t_i)$ are the computed and measured data, respectively.

The bias indicator was computed as:

$$Bias = \frac{1}{N} \sum_{i=1}^{N} (X_{mod}(t_i) - X_{obs}(t_i))$$

where N is the number of samples and $X_{mod}(t_i)$ and $X_{obs}(t_i)$ are the computed and measured data, respectively. Positive bias means that the model overestimates the *in situ* data, whereas negative bias means that the model underestimates the *in situ* data.

A qualitative comparison between daily remotely sensed images of SST from MODIS Aqua and Terra satellite and first-layer water temperature were performed.

Once Exp#1 was validated, outputs for July-August 2009-2018 were used to calibrate and validate Exp#2, where the model was forced with climatological conditions (Figure 5). For this purpose, an average water temperature for the first layer was calculated for both Exp#1 and Exp#2 and compared.

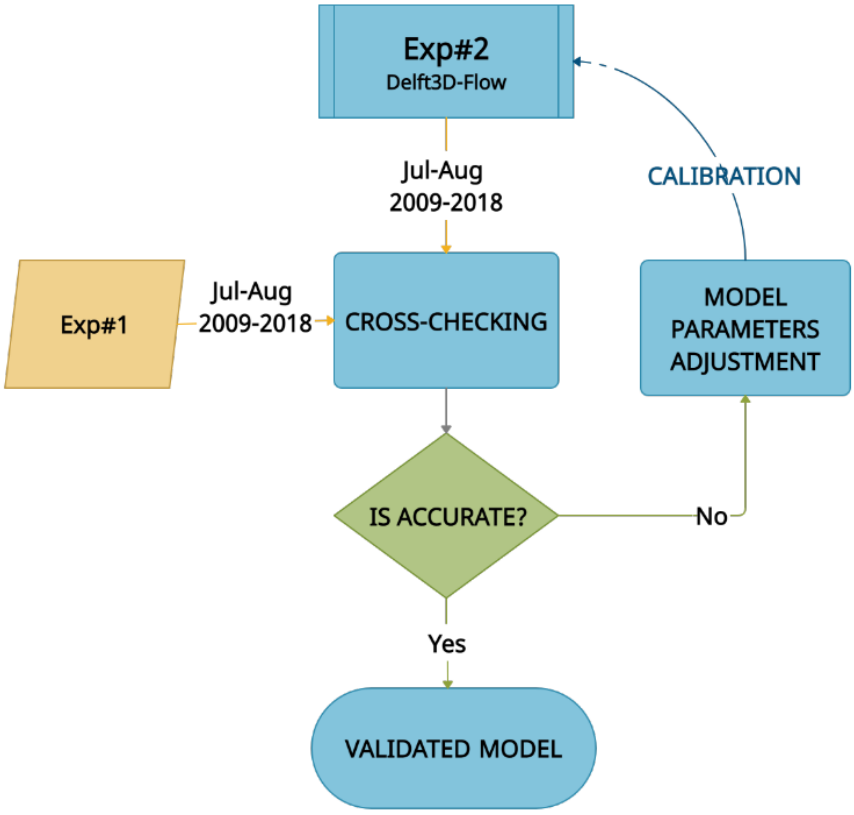

Figure 5. Validation and calibration method of the model forced with climatological data (Exp#2).

2.2.5. Processing of numerical data

The first-layer seawater temperature computed by the model was prescribed as input to the species distribution model (Figure 3). Additionally, computed water level, salinity and top-layer temperature (Exp#1) were used to calibrate and validate the model in reproducing accurately flow and transport conditions.

2.3. Species distribution model (SDM)

The species distribution model used in this work was previously defined and validated by Des et al. (2020b) for *H. elongat*a and *B. bifurcata* in the Rías Baixas, south of the study area. This species distribution model is based on the thermal survival threshold of adult fronds of *H. elongata* (18 ºC) and *B. bifurcata* (24.7 ºC) determined by Martínez et al. (2015) using tank experiments, and defines lethal conditions when daily mean SST overpass the survival threshold of each specie during at least 10 consecutive days.

SST outputs of Exp#2 were used as input of the SDM, obtaining **habitat thermal suitability maps** for both species for the historical (1999-2018) and future (2080-2099) periods. The habitat suitability maps represent the presence/absence of populations based on the percentage of time under lethal conditions, following the classification proposed by Des et al. (2020b). Optimal conditions (P1) are considered when the percentage of time under lethal conditions is less than 11%. For intermediate conditions (P2), the occurrence of lethal conditions is between 11 and 22 %. Under sub-lethal conditions (P3), the area is in lethal conditions 22% to 33% of the time. Absence means that lethal conditions occur more than 33 % of the time. **Favorability maps** were also calculated, depicting the areas where *H. elongata* and *B. bifurcata may* coexist, those where the water temperature is only favorable for *B. bifurcata,* and those unfavorable for both species.

3. Results

3.1. Hydrodynamic model validation

As a result of the calibration process, the same model's parameterization was obtained for Exp#1 and Exp#2 (Table 2). This parameterization offers the best fit between the Exp#1 outputs and the measured data and between Exp#2 and Exp#1, which comparisons are shown below.

Table 2. Parameterisation of the DELFT3D-Flow model.

Parameter	Specification
Bottom roughness	Manning's formula.
	Constant Manning´s roughness coefficient of 0.024
Horizontal eddy viscosity	500-5 $m^2 s^{-1}$
Horizontal eddy diffusivity	5 $m^2 s^{-1}$
Vertical eddy viscosity	0.0001 $m^2 s^{-1}$
Vertical eddy diffusivity	0.0001 $m^2 s^{-1}$
Heat flux model	Absolute flux, net solar radiation
Wind	Space varying wind and pressure
Turbulence closure	k-ε
Time step	0.5 min

3.1.1. Exp#1validation

The computed and observed sea surface elevation at four tidal stations (A Coruña 2, Ferrol 1, Ferrol 2 and Langosteira) for 30 days is depicted in Figure 6. The computed tidal elevation closely follows the observed records during the spring-neap tidal cycle, showing that the numerical model is able to reproduce the tidal propagation. The average RMSE and the predictive skill are 0.09 and 0.99 respectively. Individual values are depicted in Figure 6.

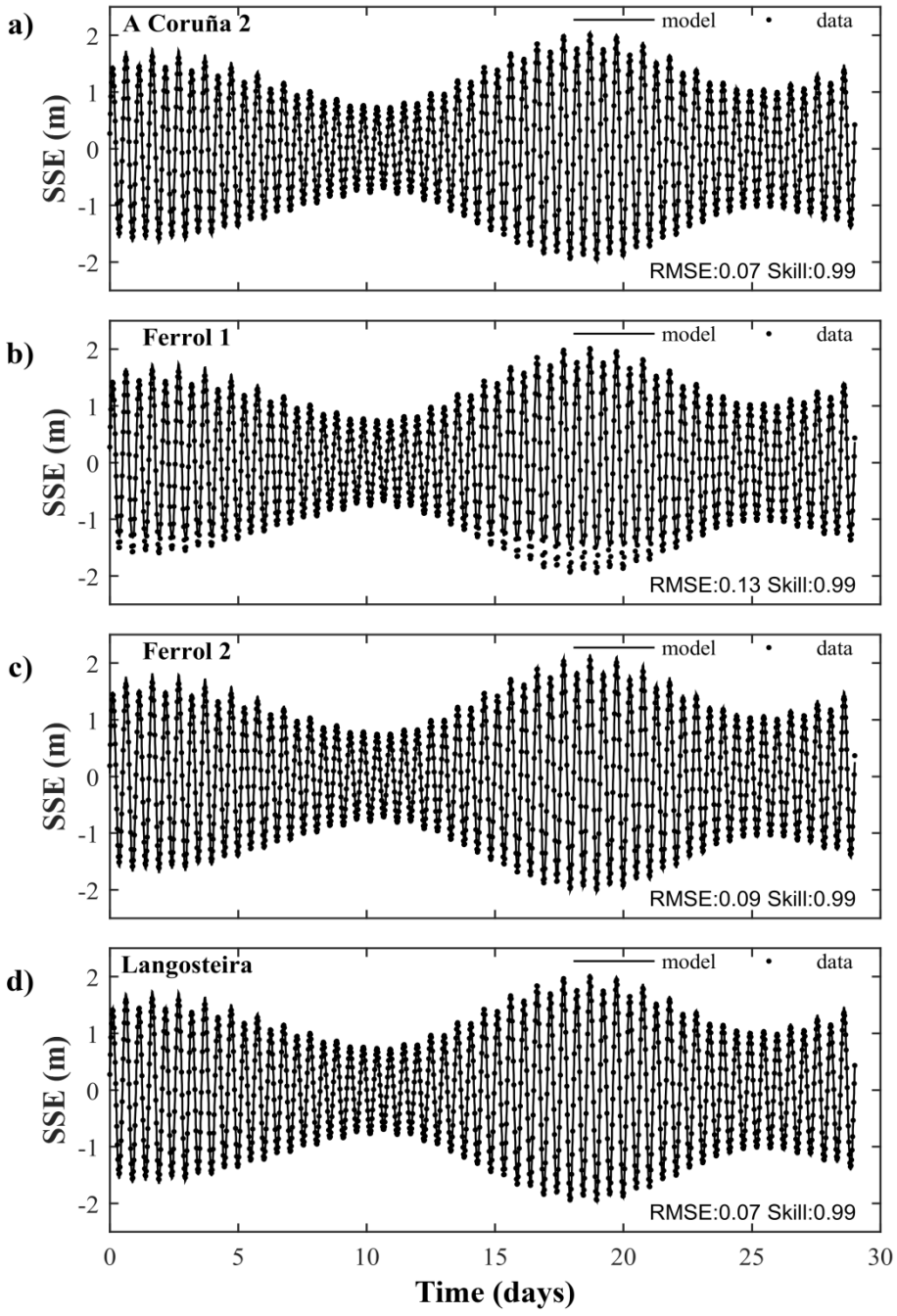

Figure 6. Comparison between observed (dots) and computed (solid lines) Sea Surface Elevation (SSE) at a) A Coruña 2, b) Ferrol 1, c) Ferrol 2, d) Langosteira tidal gauge stations during July 2015 (30 days).

Differences between amplitude and phase for the main computed and observed tidal harmonic constituents (M_2, S_2, O_1 and K_1) at four tidal stations (A Coruña 2, Ferrol 1, Ferrol 2 and Langosteira) are shown in Table 3. Comparison of the main semidiurnal tidal constituent (M_2) shows an average difference of about 2 cm in amplitude. At A Coruña 2,

Ferrol 1 and Langosteira tidal stations, the phase difference ranges from 0.52 to 0.69º, which means an average delay of 1.3 min; however, for Ferrol 2 tidal station, the difference reaches 2.96º (6.13 min of delay).

Table 3. Model accuracy in reproducing the main tidal harmonic constituent (M2, S2, O1 and K1) measured at A Coruña 2, Ferrol 1, Ferrol 2 and Langosteira tide gauge stations.

Main harmonic constituent	Tide gauge	Amplitude (m)			Phase (°)		
		Field	Model	Difference	Field	Model	Difference
M_2	A Coruña 2	1.22	1.22	0.00	86.45	86.97	0.52
	Ferrol 1	1.22	1.16	-0.06	86.98	87.67	0.69
	Ferrol 2	1.24	1.24	0.00	88.93	91.89	2.96
	Langosteira	1.21	1.21	-0.01	85.98	86.65	0.68
S_2	A Coruña 2	0.40	0.42	0.02	128.69	130.14	1.45
	Ferrol 1	0.40	0.37	-0.03	129.02	130.36	1.35
	Ferrol 2	0.40	0.42	0.02	132.13	136.83	4.70
	Langosteira	0.40	0.42	0.02	128.58	129.83	1.25
O_1	A Coruña 2	0.05	0.06	0.01	325.23	324.95	-0.29
	Ferrol 1	0.05	0.06	0.00	325.72	333.27	7.54
	Ferrol 2	0.06	0.06	0.01	326.93	328.92	1.99
	Langosteira	0.05	0.06	0.01	324.85	325.21	0.36
K_1	A Coruña 2	0.08	0.11	0.03	88.23	87.94	-0.29
	Ferrol 1	0.08	0.10	0.02	88.11	92.10	3.99
	Ferrol 2	0.08	0.11	0.03	89.81	90.75	0.94
	Langosteira	0.08	0.11	0.03	82.64	87.38	4.74

Statistical analysis of the model's accuracy in reproducing near-surface water temperature shows a RMSE of 0.73 ºC and a σ of 0.82 ºC at Villano Sisargas buoy. At Langosteira buoy the obtained RMSE and σ for water temperature were 0.95 ºC and 1.56 ºC, respectively. The bias is positive for both buoys, with a value of 0.41 ºC at Langosteira and nearly zero at Villano Sisargas. The modelled and measured near-surface water temperature at Langosteira buoy is depicted in Figure 7, showing that both data series follow a similar pattern, with slightly higher modelled values and indicates that Exp#1 overestimates near-surface water temperature. Comparing modelled and *in* situ salinity data for Villano Sisargas buoy (Langosteira buoy have no available salinity data) shows a RMSE of 0.05, a σ of 0.03 and no bias was obtained (Table 4).

Table 4. Model accuracy in reproducing near-surface water temperature and salinity measured at Villano Sisargas and Langosteira buoys for July-August 2015.

Buoy	Near-surface water temperature (°C)			Near-surface salinity		
	RMSE	Standard Deviation (σ)	Bias	RMSE	Standard Deviation (σ)	Bias
Villano Sisargas	0.73	0.82	0.04	0.05	0.03	0.00
Langosteira	0.95	1.56	0.41	-	-	-

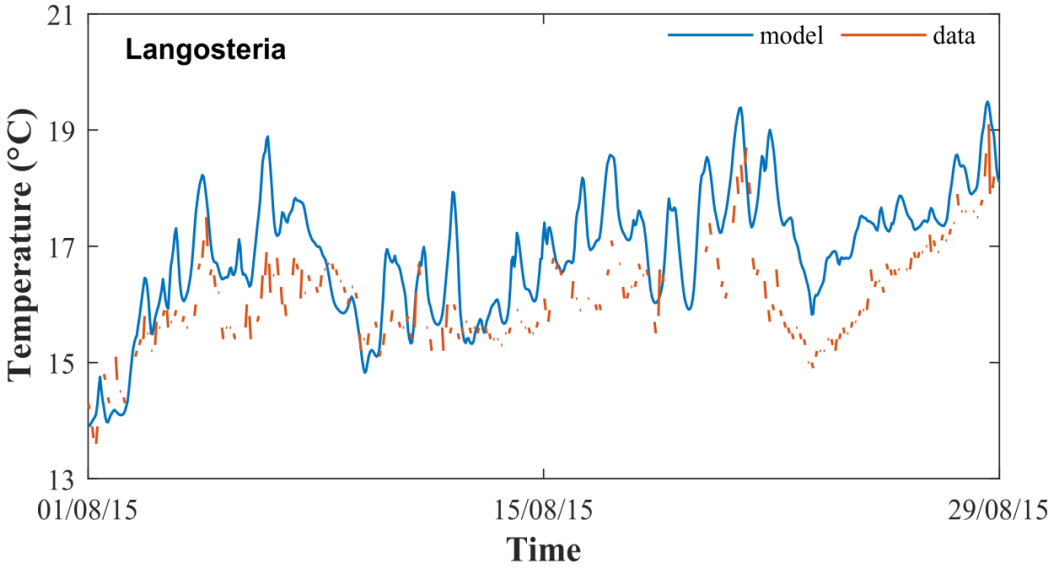

Figure 7. Comparison between observed (solid orange lines) and computed (solid blue lines) near-surface water temperature (at 3 m depth) from the Langosteira buoy for August 2015.

Modelled and observed SST show a similar pattern. An example of this comparison is shown in Figure 8, where the modelled (Figure 8a) and measured (Figure 8b) SST for 20th August 2015 are depicted. Both datasets show SST reaching approximately 20°C in the deep areas of the open sea and decreasing towards the coastal areas. The lowest SST values (around 17°C) are observed in the southwest and northwest coastal areas. SST values around 19°C are observed in the bay located between Sisargas Islands and A Coruña (nearly 2°C more than the lowest nearshore values). Additionally, modelled water temperature shows that SST can reach 21°C in shallow areas at the innermost parts of the rias of Ares-Betanzos and Ferrol.

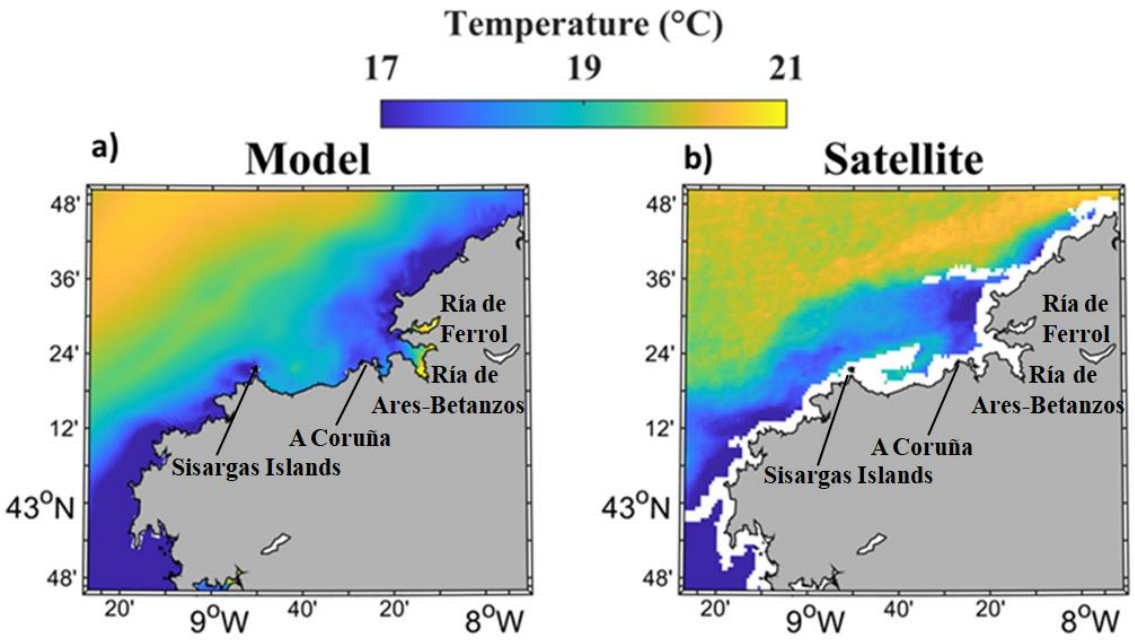

Figure 8. Sea surface temperature retrieved from the model results (a) and satellite imagery (b) on 20th August 2015.

The model ability to reproduce vertical profiles of salinity and water temperature is summarised in Table 5. The analysis of water temperature shows that the mean RMSE obtained for the Ría of Ares-Betanzos is 0.80 ºC, with a σ of 0.36 and 0.30±0.19 for salinity. The bias is positive but almost zero for water temperature (0.02 ºC) and positive for salinity (0.27).

Table 5. Model accuracy in reproducing *in situ* vertical profiles of water temperature and salinity calculated averaging the values obtained for each sampling station (L1, L2, L3 and L4) for July-August 2015.

Sampling Station	Temperature (°C)			Salinity		
	RMSE	Standard Deviation (σ)	Bias	RMSE	Standard Deviation (σ)	Bias
L1	0.69	0.32	-0.17	0.11	0.07	0.09
L2	0.81	0.29	0.13	0.20	0.21	0.18
L3	0.94	0.40	0.02	0.46	0.22	0.44
L4	0.74	0.43	0.10	0.42	0.24	0.37
Mean	0.80	0.36	0.02	0.30	0.19	0.27

A modelled vs *in situ* water temperature (Figure 9a) and salinity (Figure 9b) vertical profiles have been plotted as an example for visual comparison. Both profiles show that the model is capable of adequately reproducing the transport conditions in the water column. The analysis of water temperature profiles (Figure 9a) shows that the model underestimates water temperature at surface layers and overestimates it at lower layers. Regarding salinity (Figure 9b), the model overestimates measured data along the entire water column.

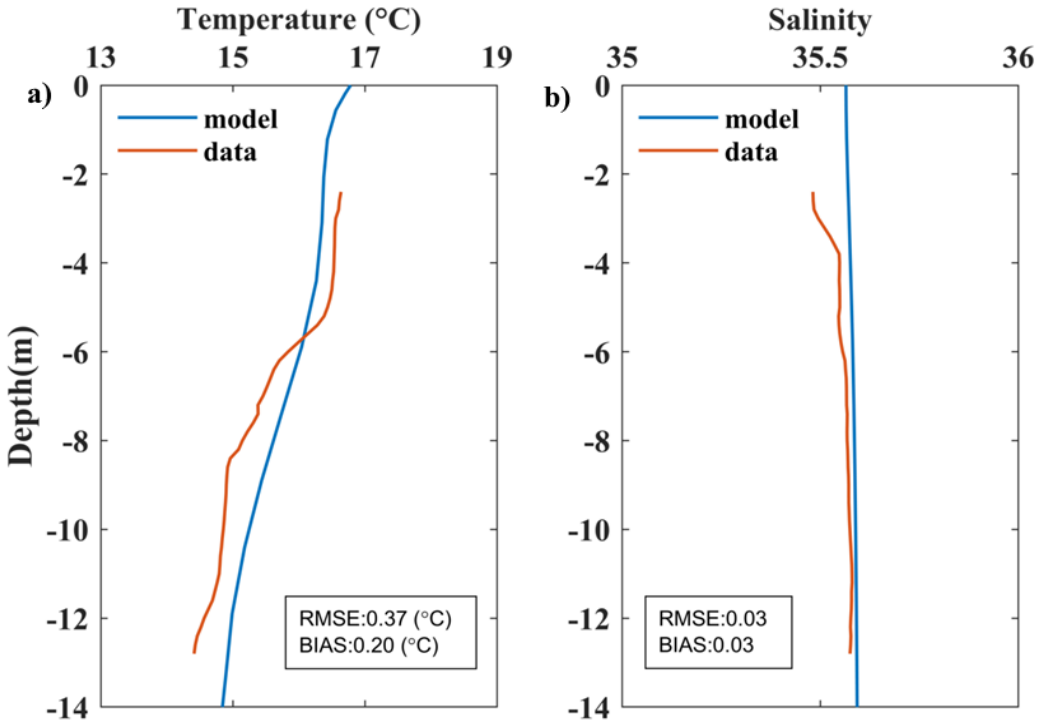

Figure 9. Water temperature (a) and salinity (b) vertical profiles modelled (blue line) and measured (orange line) at the sampling station L1 on 03/08/2015 and on 10/08/2015, respectively.

3.1.2. Exp#2 validation

The maps of average top-layer water temperature calculated over the period July-August 2009-2018 using realistic (Exp#1, Figure 10a) and climatological (Exp#2, Figure 10b) data as model's input show a similar pattern, with higher top-layer water temperature values offshore decreasing landwards. The difference map ($\Delta T = T_{Exp\#2}-T_{Exp\#1}$, Figure 10c) reveals that, in general, Exp#2 underestimates top-layer temperature related to Exp#1. The most significant differences are observed in the oceanic area, with values near -2 ºC. However, the difference is almost zero nearshore (Figure 10c).

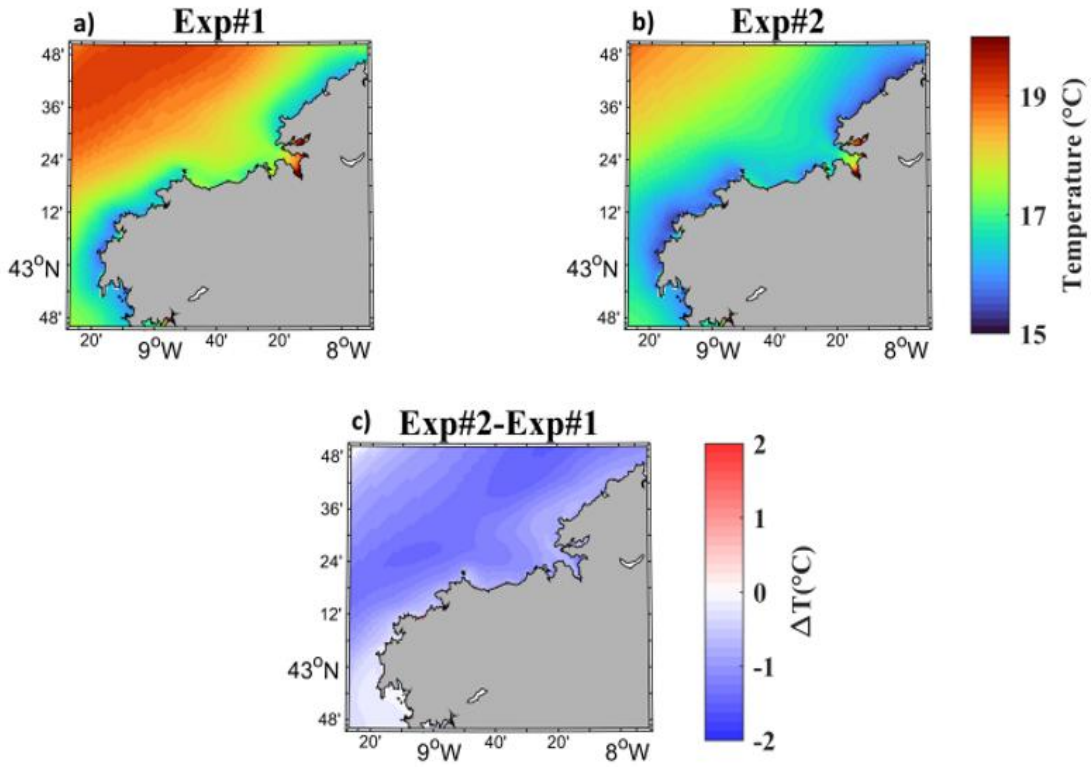

Figure 10. Predicted average water temperature (upper layer) using Exp#1 (a), Exp#2 (b) and the difference between them ($\Delta T = T_{Exp\#2}-T_{Exp\#1}$, c) over the period July-August 2009-2018.

3.2. Thermal habitat suitability and favorability maps

Habitat suitability map for *H. elongata* performed for the historical period (Figure 11) reveals that the thermal conditions are favorable for the presence of this alga along most of the study area. The areas where thermal conditions are optimal (P1) occupy almost all the coast. Thermal suitability for *H. elongata* decreases in the rias of Ferrol and Ares-Betanzos, where intermediate conditions (P2) are observed in the external areas and sub-lethal (P3) and lethal conditions (Absence) in the middle area of the rias of Ares-Betanzos and Ferrol. Small isolated spots of lethal conditions are also observed along the shoreline.

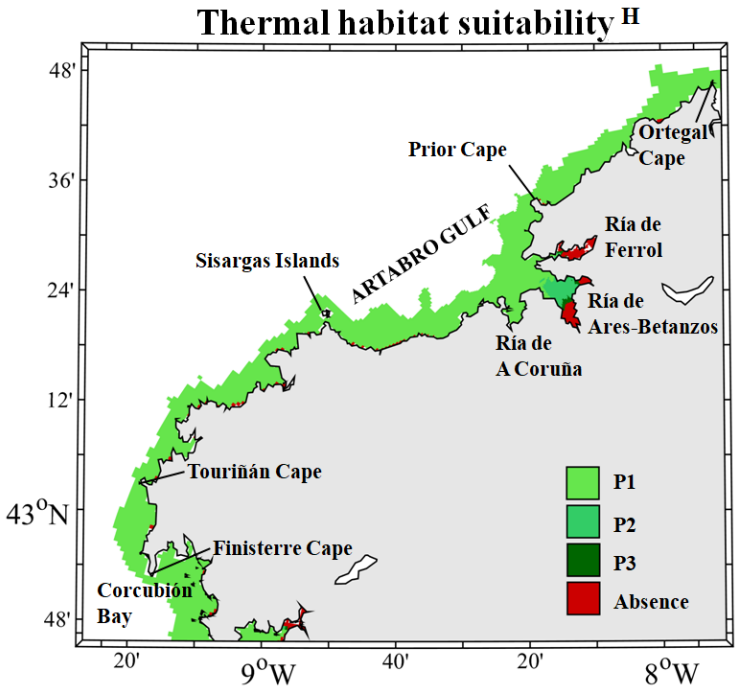

Figure 11. Thermal habitat suitability map for *H. elongata* based on simulated SST for the historical period (July-August 1999-2018) using Exp#2. P1 represents optimal conditions, P2 intermediate conditions, P3 sub-lethal conditions and Absence lethal conditions.

By the end of the century, areas where thermal conditions are lethal for *H. elongata* may widely increase (Figure 12). Lethal conditions are observed from the Corcubión Bay to the Artabro Gulf. From Touriñán Cape to Sisargas Islands, absence occurs nearshore, becoming sub-lethal (P3) and intermediate (P2) moving offshore. To the north of the study area, thermal conditions are mainly favorable to the presence of *H. elongata*.

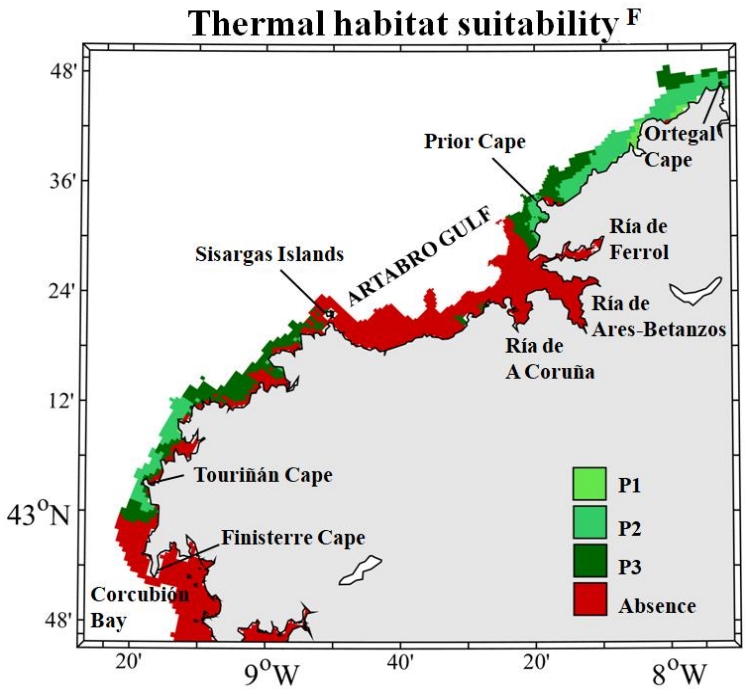

Figure 12. Thermal habitat suitability map for *H. elongata* based on simulated SST for the future period (July-August 2080-2099) using Exp#2. P1 represents optimal conditions, P2 intermediate conditions, P3 sub-lethal conditions and Absence lethal conditions.

In the case of *B. bifurcata*, historical (Figure 13) and future (Figure 14) habitat suitability maps are similar. In both cases, the study area is thermally optimal for the presence of *B. bifurcata*. Only absence is predicted in a small area in the innermost part of the Ría de Ares-Betanzos by the end of the century.

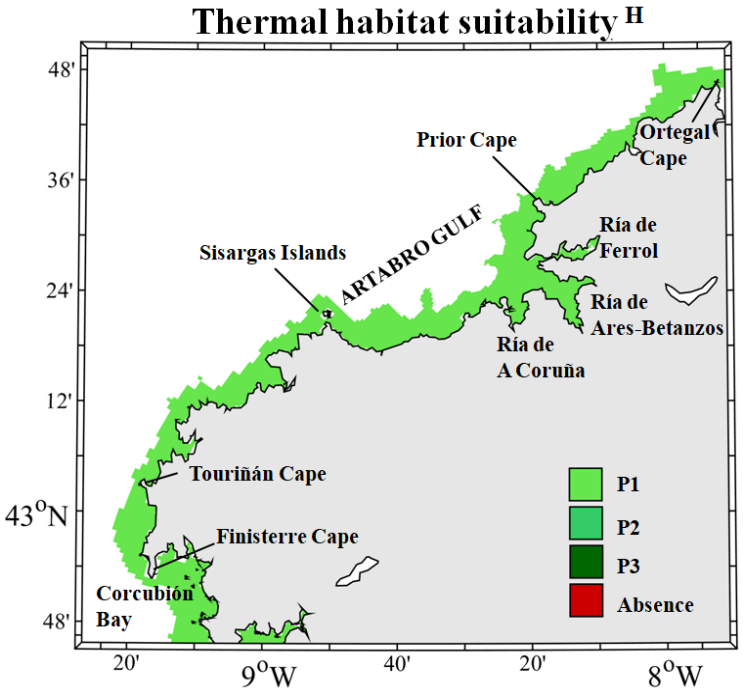

Figure 13. Thermal habitat suitability map for *B.bifurcata* based on simulated SST for the historical period (July-August 1999-2018) using Exp#2. P1 represents optimal conditions, P2 intermediate conditions, P3 sub-lethal conditions and Absence lethal conditions.

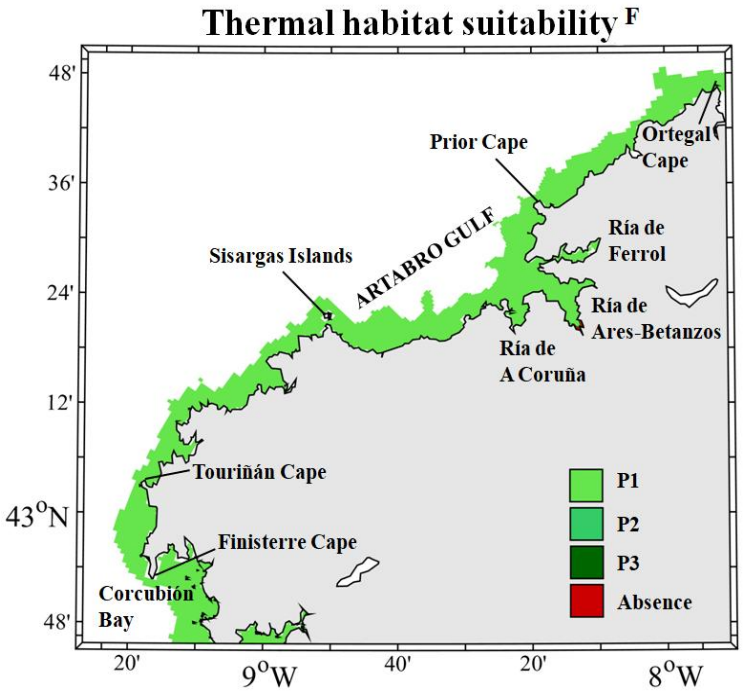

Figure 14. Thermal habitat suitability map for *B. bifurcata* based on simulated SST for the future period (July-August 2080-2099) using Exp#2. P1 represents optimal conditions, P2 intermediate conditions, P3 sub-lethal conditions and Absence lethal conditions.

Regarding historical favorability map, the coexistence of *H. elongata* and *B. bifurcata* can occur in most of the study area (Figure 15), except for the innermost part of the rias of Ferrol and Ares-Betanzos, where thermal conditions are favorable to the presence of *B. bifurcata* and the absence of *H. elongata*.

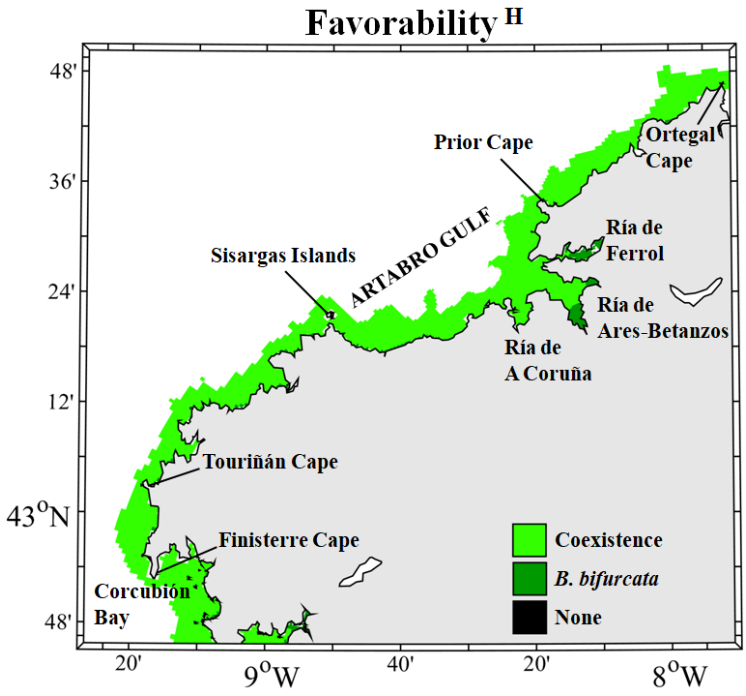

Figure 15. Favorability map for *H. elongata* and *B. bifurcata* for the historical period (July–August 1999–2018).

Favorability map for the future period (Figure 16) reveals that the coexistence area for both species could be reduced to the northern part of the study area and some scattered spots. Most of the coast may be thermally favorable only for the presence of *B. bifurcata*. The absence of both species only occurs in the innermost part of the Ría de Betanzos.

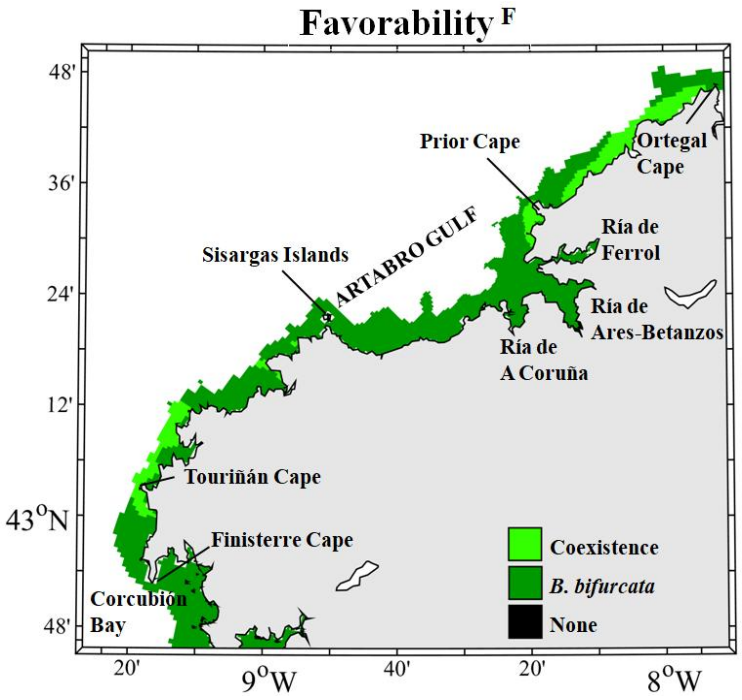

Figure 16. Favorability map for *H. elongata* and *B. bifurcata* for the future period (July–August 2080–2099).

4. Discussion

Predicting the possible effects of climate change is a necessary but difficult task. Numerical models are a useful tool to carry out this task since they allow projecting different scenarios and analyzing how changes in radiative forcing may affect different systems. The geographical distribution of the species under analysis (*H. elongata* and *B. bifurcata*) is mainly correlated with SST (Lüning, 1990; Martínez et al., 2012); hence, the projected SST can be used as a predictive variable to study de possible effects of climate change on the geographical distribution of these macroalgae.

4.1. Hydrodynamic model accuracy

Following the categorization proposed by Dias et al. (2009), results of water level validation show a very good agreement between modelled and *in situ* data, proving the model's ability to reproduce water level and tidal propagation accurately. The main error is observed in reproducing tidal propagation at Ferrol 2 tidal station, where a lag of 6.13 min is observed. This difference may be derived from the presence of the Strait of Ferrol near the ria mouth, which is a very narrow channel connecting the ria with the shelf where tidal velocities increase significantly (deCastro et al., 2004). However, despite obtaining values higher than in the rest of the tide stations, the results can be considered good following the same categorization, in agreement with those obtained by Dias et al. (2009) in Ría Formosa (Portugal), Sousa et al. (2018) in the main estuaries of the NW Iberian Peninsula coast and Des et al. (2019) in the Rías Baixas. Nevertheless, some improvements to the model could be considered in order to better reproduce the tidal propagation inside the Ría de Ferrol. On the one hand, calibration parameters of the numerical model could be adjusted in the area, especially the bottom roughness, to modify the turbulence generated by shear at the bed. On the other hand, the resolution in the Strait of Ferrol could be increased. This area is currently represented by four grid cells of approximately 150 × 150 m and may not accurately reproduce the channel topography.

The validation of transport conditions for Exp#1 shows results similar to those obtained by Des et al. (2019, 2020a, 2020b) using Delft3D-Flow model, Cerralbo et al. (2013) using

ROMS model and Sousa et al. (2014a, 2014b, 2018) using MOHID model, all of them for the Rías Baixas, located south of the study area. Regarding water temperature, the analysis of near-surface water temperature shows a positive bias of 0.41 °C at the Langosteira buoy and no bias at Villano Sisargas (Table 4). Additionally, the comparison between satellite and modelled SST data showed the ability of the model to reproduce SST patterns, observing a positive bias, in agreement with previous results by Sousa et al. (2018). Regarding vertical profiles, positive bias is also obtained. All these results indicate that the model tends to overestimate the water temperature.

Regarding the ability of Exp#2 to reproduce transport conditions, the comparison of top-layer water temperature modelled by using Exp#1 and Exp#2 shows that Exp#2 tends to underestimate Exp#1 top-layer temperature less than 1°C (Figure 10), showing a good agreement between both sets of data. Considering that Exp#1 slightly overestimates *in* situ data, it can be suggested that Exp#2 shows a close pattern related to the measured data.

The main limitations of numerical models are the quality and the resolution of the input data since the model will propagate the errors. In the case of the resolution of the input data, both models, the Atlantic-Iberian Biscay Irish-Ocean Physics Reanalysis and MOHC-HadGEM2-Es covered a large area with a coarse temporal and spatial resolution. Additionally, a large amount of data from different sources was used in this work, both as input to the numerical model and for calibration purposes. Data have an associated error that must also be taken into account. Nevertheless, results obtained in the validation processes demonstrate the model accuracy in reproducing the hydrodynamics of the study area under realistic and climatological conditions. Finally, it is necessary to highlight that despite Delft3D-Flow shows excellent results to simulate real ecosystems (Grunnet et al., 2004; Sutherland et al., 2004; Iglesias and Carballo, 2009, 2010a, 2010b), models only represent an approximation to reality.

4.2. Thermal habitat suitability

During the historical period, numerical simulations show that thermal conditions are suitable for the presence of *H. elongata* (Figure 11) in most locations along the study area. Absences are observed in the inner areas of the rias of Ferrol and Ares-Betanzos and some spots along the shore. These results are consistent with record-based distribution maps performed by Martinez et al. (2012), who registered presences and absences at the same areas and validated the use of the mechanistic distribution model for the study area. The use of this model indicates that the geographical distribution of *H. elongata* may be reduced by more than half by the end of the century under a RCP 8.5 scenario compared to the historical one. However, the projections do not show remarkable changes for *B. bifurcata* population.

Thermal habitat suitability maps, mainly thermal suitability map for *H. elongata* under future conditions, show a relation with upwelling patterns in the area. The unfavorable thermal conditions observed in the inner areas of the rias of Ferrol and Ares-Betanzos for *H. elongata* during historical period (Figure 11) may be related to the fact that the upwelled water does not reach these rias due to the morphology of the Artabro Gulf, the area confined by Sisargas Isles and Prior Cape (Prego and Varela, 1998). For the future period (Figure 12), thermal conditions for *H. elongata* are projected to worsen due to ocean warming. This worsening appears to be mitigated by the coastal upwelling since the areas where the species could inhabit are closely linked to the areas where the upwelling water reaches the surface. In the Artabro Gulf and around Corcubion bay, *H. elongata* may become extinct by the end of the century. Prego and Bao (1997) indicated that upwelling located near the north of Finisterre Cape is discontinuous and remains distant form the coast (near the edge of the continental shelf), which may explain the predominance of lethal conditions nearshore from Touriñán Cape to Sisargas Islands (Figure 12) and the improvement of habitat suitability moving offshore. Most suitable conditions (optimal and intermediate) were found from Prior Cape to Ortegal Cape, where coastal upwelling occurs (Prego and Varela, 1998) promoting surface water cooling. These results are consistent with previous studies which indicated that the upwelling areas could act as refugia for many species (Lourenco et al., 2016; Duarte and Viejo, 2018) since they have a lower

tendency to warming than the near ocean and adjacent coastal areas (Alvarez et al., 2009; Santos et al., 2011, 2012; Varela et al., 2018; Seabra et al., 2019). Several studies have detected a faster decline of *H. elongata* , and macroalgae with similar thermal threshold, north of the study area, in the northern coast of the Iberian Peninsula (Martinez et al., 2012; Duarte et al., 2013; Casado-Amezúa et al., 2019), projecting even the extinction of these species (Martinez et al., 2012, 2015). Martinez et al. (2012) relates this decline with the absence of upwelling events in the region, having consequently higher SST (Gómez-Gesteira et al., 2008; Alvarez et al., 2012) that lead to lethal conditions at a faster rate (Fernández 2016). Martinez et al. (2012) and Des et al. (2020b) indicate that the Rías Baixas, south of the study area, act as contemporary refugia for *H. elongata*, agreeing with the results of the present study. Des et al. (2020b) performed numerical simulations for the Rías Baixas covering the same period as those carried out in this study and projected the extinction of *H. elongata* in the Rías Baixas by the end of the century. However, the results of the present study project that this species, and those with a similar thermal tolerance threshold, could continue to inhabit some regions of the study area. Despite both areas are affected by upwelling, coastal physiography is very different, changing upwelling and circulation patterns and, therefore, the response to ocean warming. Upwelling favorable winds are expected to increase intensely (Bakun, 1990; Casabella et al., 2014; Sousa et al., 2017), but this increase in the upwelling index may not be directly reflected in the effectiveness of the upwelling (Sousa et al., 2020). These authors analyzed the effectiveness of the upwelling favorable winds by the end of the century (2070-2099) along the Northwest Iberian Peninsula under a RCP8.5 scenario, concluding that in the future upwelling will be less effective in the Rías Baixas than in the area of study of the present work. For the study area of the present work, Sousa et al. (2020) projected no significant changes in the Artabro Gulf, a slight increase from Finisterre Cape to Sisargas Islands and a slight decrease inside of Corcubion Bay. They do not have projections from Prior Cape to Ortegal Cape. These authors attribute the changes in upwelling effectiveness to increased stratification, which was also observed by Des et al. (2020b) for the Rías Baixas. Thus, changes in stratification and upwelling effectiveness may explain the differences between projections performed for Rías Baixas, predicting the extinction of *H. elongata* by the end

of the century (Des et al., 2020b), and the results obtained in this work, where local refugia for this species are projected mainly from Prior Cape to Ortegal Cape.

In the case of *B. bifurcata*, optimal conditions were shown along the study area for the present and future periods (Figure 13 and Figure 14), with absence areas in the innermost southern part of the Ría de Ares-Betanzos for this last period. Projected ocean warming may not impact the geographical distribution of this alga and the study area may still act as potential contemporary refugia for *B. bifurcata* and another warm-temperate species with a similar tolerance limit. These results are in accordance with those obtained by Martinez et al. (2015), who observed the presence of this species along the area of study in a survey conducted from 2004 to 2006 and also predicted a future increase in abundance. Similar results were obtained by Des et al. (2020b) for the Rías Baixas. These authors determined that thermal conditions are favorable for the presence of *B. bifurcata* both in the historical period and in the future. Additionally, a similar trend was shown by Ramos et al. (2020) in a study along the north and northwest coast of the Iberian Peninsula in 2011 and 2017, finding that *B.bifurcata*, and other warm-temperate seaweeds such as *Coralline algae* and *Cystoseira baccata* increased in abundance probably due to ocean warming.

Currently, both species, *H. elongata* and *B. bifurcata*, may coexist in almost the entire study area (favorability maps, Figure 15). However, the range contraction of *H. elongata*, and cold-temperate species due to ocean warming, may shift the geographical distribution of the macroalgae in the future and favour the dominance of *B. bifurcata* and other warm-temperate species (Figure 16). The significant retraction of cold-temperate intertidal seaweeds is not limited to the study area. New estimates reveal a global decline of kelp population at a rate of ~ 2% per year over the past half century (Wernberg et al., 2019). In most cases, the retraction was caused by ocean warming and marine heat waves (IPCC, 2019). It is estimated that 43% loss of kelp forests disappeared from ~100km of coastline in Western Australia after an extreme marine heat wave in 2011 and were replaced by seaweeds characteristic of subtropical waters (Wernberg et al., 2016). Model projections also support that the observed range contraction of kelp forests will likely continue at rapid rates at the lower latitudinal limit of geographic distribution under the RCP 8.5 scenario

(Assis et al., 2018; IPCC, 2019), as this study shows for *H. elongata* in the northwestern corner of the Iberian Peninsula.

In addition to ocean warming, seaweeds are affected by others stressors such as coastal eutrophication, acidification and pollution, which are deteriorating even more macroalgae populations (Fairweather, 1990; Díez et al., 2009).

The present study analyses the geographical distribution of two representative macroalgae by analyzing heat waves driven by SST. Although SST is the main factor affecting the geographical distribution of these species, there are other important factors such as air temperature, wave exposure, and substrate type (Martínez et al., 2012). The inclusion of these factors in the study could help to better understand how climate change will impact the habitat-former species.

5. Conclusions

The **main objective of the present work** was to analyze the potential effects of climate change, under the RCP 8.5 scenario, on the geographical distribution of two foundation habitat-forming macroalgae (*H. elongata* and *B. bifurcata*) from Corcubion Bay to Ortegal Cape by performing a downscaling of the GCMs using the numerical model Delf3D-Flow.

The main conclusions obtained can be summarized as follows:

- The implementation, validation and calibration of Delf3D-Flow performed in this work provide an accurate representation of the hydrodynamics of the study area, both under realistic and climatological conditions, allowing making future projections.
- Thermal conditions are, in general, favorable for the presence of *H. elongata* and *B. bifurcata* in the study area during the historical period.
- By the end of the century, a significant decline of *H. elongata* and other cold-temperate seaweeds populations may occur in the Artabro Gulf and from Corcubion Bay to Sisargas Island.
- Coastal areas from Prior Cape to Ortegal Cape may be climatic refugia for *H. elongata* and other cold-temperate macroalgae, preventing their local extinction.
- Most of the study area may be thermally favorable for the settlement of *B. bifurcata* and other warm-temperate affinity seaweeds by the end of the century.
- Both species mostly coexist along the study area during the historical period. However, by the end of the century, *H. elongata* and other cold-temperate seaweeds populations may decline, and *B. bifurcata* and other warm-temperate affinity seaweeds may occupy the left space. Both types may coexist only in a few spots.
- The geographical distribution of these seaweeds seems to be related to the upwelling patterns of the study area.

References

Alvarez, I., Ospina-Alvarez, N., Pazos, Y., deCastro, M., Bernardez, P., Campos, M.J., Gomez-Gesteira, J.L., Alvarez-Ossorio, M.T., Varela, M., Gomez-Gesteira, M., Prego, R., 2009. A winter upwelling event in the Northern Galician Rias: Frequency and oceanographic implications. Estuar. Coast. Shelf Sci. 82, 573–582. https://doi.org/10.1016/j.ecss.2009.02.023.

Alvarez, I., Ospina-Alvarez, N., Decastro, M., Varela, M., Gomez-Gesteira, M., Prego, R., 2010. Poleward intrusion in the northern Galician shelf. Estuar. Coast. Shelf Sci. 87, 545–552. https://doi.org/10.1016/j.ecss.2010.02.009.

Alvarez, I., Lorenzo, M.N., deCastro, M., 2012. Analysis of chlorophyll a concentration along the Galician coast: seasonal variability and trends. ICES J. Mar. Sci. 69, 728–738. https://doi.org/10.1093/icesjms/fss045.

Ashcroft, M.B., 2010. Identifying refugia from climate change. J. Biogeogr. 37, 1407–1413. https://doi.org/10.1111/j.1365-2699.2010.02300.x.

Assis, J., Araújo, M.B., Serrão, E.A., 2018. Projected climate changes threaten ancient refugia of kelp forests in the North Atlantic. Glob. Change Biol. 24, e55–e66. https://doi.org/10.1111/gcb.13818.

Bakun, A., 1990. Global Climate Change and Intensification of Coastal Ocean Upwelling. Science 247, 198–201. https://doi.org/10.1126/science.247.4939.198.

Beaugrand, G., Edwards, M., Brander, K., Luczak, C., Ibanez, F., 2008. Causes and projections of abrupt climate-driven ecosystem shifts in the North Atlantic. Ecol. Lett. 11, 1-12. https://doi.org/10.1111/j.1461-0248.2008.01218.x.

Bennett, S., Wernberg, T., Connell, S.D., Hobday, A.J., Johnson, C.R., Poloczanska, E.S., Bennett, S., Wernberg, T., Connell, S.D., Hobday, A.J., Johnson, C.R., Poloczanska, E.S., 2015. The 'Great Southern Reef': social, ecological and economic value of Australia's neglected kelp forests. Mar. Freshw. Res. 67, 47–56. https://doi.org/10.1071/MF15232.

Bindoff, N.L., Cheung, W.W.L., Kairo, J.G., Arístegui, J., Guinder, V.A., Hallberg, R., Hilmi, N.J.M., Jiao, N., Karim, M.S., Levin, L., O'Donoghue, S., Purca Cuicapusa, S.R., Rinkevich, B., Suga, T., Tagliabue, A., Williamson, P., 2019. Changing Ocean, Marine Ecosystems, and Dependent Communities, in: Pörtner, H.-O., Roberts, D.C., Masson-Delmotte, V., Zhai, P., Tignor, M., Poloczanska, E., Mintenbeck, K., Alegría, A., Nicolai, M., Okem, A., Petzold, J., Rama, B., Weyer, N.M. (Eds.), IPCC Special Report on the Ocean and Cryosphere in a Changing Climate. Intergovernmental Panel on Climate Change, Switzerland, pp. 477–587.

Brown, P.T., Caldeira, K., 2017. Greater future global warming inferred from Earth's recent energy budget. Nature 552, 45–50. https://doi.org/10.1038/nature24672.

Burrows, M.T., Schoeman, D.S., Buckley, L.B., Moore, P., Poloczanska, E.S., Brander, K.M., Brown, C., Bruno, J.F., Duarte, C.M., Halpern, B.S., Holding, J., Kappel, C.V., Kiessling, W., O'Connor, M.I., Pandolfi, J.M., Parmesan, C., Schwing, F.B., Sydeman, W.J., Richardson, A.J., 2011. The Pace of Shifting Climate in Marine and Terrestrial Ecosystems. Science 334, 652–655. https://doi.org/10.1126/science.1210288.

Carballo, R., Iglesias, G., Castro, A., 2009a. Numerical model evaluation of tidal stream energy resources in the Ría de Muros (NW Spain). Renew. Energy 34, 1517–1524. https://doi.org/10.1016/j.renene.2008.10.028.

Carballo, R., Iglesias, G., Castro, A., 2009b. Residual circulation in the Ría de Muros (NW Spain): A 3D numerical model study. J. Mar. Syst. 75, 116–130. https://doi.org/10.1016/j.jmarsys.2008.08.004.

Casabella, N., Lorenzo, M.N., Taboada, J.J., 2014. Trends of the Galician upwelling in the context of climate change. J. Sea Res., The Atlantic Iberian Margin: a research synthesis 93, 23–27. https://doi.org/10.1016/j.seares.2014.01.013.

Casado-Amezúa, P., Araújo, R., Bárbara, I., Bermejo, R., Borja, Á., Díez, I., Fernández, C., Gorostiaga, J.M., Guinda, X., Hernández, I., Juanes, J.A., Peña, V., Peteiro, C., Puente, A., Quintana, I., Tuya, F., Viejo, R.M., Altamirano, M., Gallardo, T., Martínez, B., 2019. Distributional shifts of canopy-forming seaweeds from the Atlantic coast of Southern Europe. Biodivers. Conserv. 28, 1151–1172. https://doi.org/10.1007/s10531-019-01716-9.

Cerralbo, P., Grifoll, M., Espino, M., López, J., 2013. Predictability of currents on a mesotidal estuary (Ria de Vigo, NW Iberia) | SpringerLink. Ocean Dyn 63.

deCastro, M., Gomez-Gesteira, M., Prego, R., Alvarez, I., 2004. Ria–ocean exchange driven by tides in the Ria of Ferrol (NW Spain). Estuar. Coast. Shelf Sci. 61, 15–24. https://doi.org/10.1016/j.ecss.2004.04.001.

Deltares, 2014. Delft3D-FLOW. Simulation of multi-dimensional hydrodynamic flows and transport phenomena, including sediments. User Manual. Hydro-Morphodynamics. Version: 3.15.34158, Delft3D Modeling Suite.

Des, M., deCastro, M., Sousa, M.C., Dias, J.M., Gómez-Gesteira, M., 2019. Hydrodynamics of river plume intrusion into an adjacent estuary: The Minho River and Ria de Vigo. J. Mar. Syst. 189, 87–97. https://doi.org/10.1016/j.jmarsys.2018.10.003.

Des, M., 2020. Hydrodynamics of NW Iberian Peninsula under past and future climate conditions. (Tesis doctoral). Universidade de Vigo, Galicia.

Des, M., Gómez-Gesteira, M., deCastro, M., Gómez-Gesteira, L., Sousa, M.C., 2020a. How can ocean warming at the NW Iberian Peninsula affect mussel aquaculture? Sci. Total Environ. 709, 136117. https://doi.org/10.1016/j.scitotenv.2019.136117.

Des, M., Martínez, B., deCastro, M., Viejo, R.M., Sousa, M.C., Gómez-Gesteira, M., 2020b. The impact of climate change on the geographical distribution of habitat-forming macroalgae in the Rías Baixas. Mar. Environ. Res. 161, 105074. https://doi.org/10.1016/j.marenvres.2020.105074.

Dias, J.M., Sousa, M.C., Bertin, X., Fortunato, A.B., Oliveira, A., 2009. Numerical modeling of the impact of the Ancão Inlet relocation (Ria Formosa, Portugal). Environ. Model. Softw. 24, 711–725. https://doi.org/10.1016/j.envsoft.2008.10.017.

Díez, I., Santolaria, A., Secilla, A., Gorostiaga, J.M., 2009. Recovery stages over long-term monitoring of the intertidal vegetation in the 'Abra de Bilbao' area and on the adjacent coast (N. Spain). Eur. J. Phycol. 44, 1–14. https://doi.org/10.1080/09670260802158642.

Duarte, L., Viejo, R., Martinez, B., Decastro, M., Gómez-Gesteira, M., Gallardo, T., 2013. Recent and

historical range shifts of two canopy-forming seaweeds in North Spain and the link with trends in sea surface temperature. Acta Oecologica 51, 1–10. https://doi.org/10.1016/j.actao.2013.05.002.

Duarte, L., Viejo, R.M., 2018. Environmental and phenotypic heterogeneity of populations at the trailing range-edge of the habitat-forming macroalga Fucus serratus. Mar. Environ. Res. 136, 16–26. https://doi.org/10.1016/j.marenvres.2018.02.004.

Fairweather, P.G., 1990. Sewage and the biota on seashores: Assessment of impact in relation to natural variability | SpringerLink. Environ. Monit. Assess. 14. https://doi.org/10.1007/BF00677916.

Fernández, C., 2016. Current status and multidecadal biogeographical changes in rocky intertidal algal assemblages: The northern Spanish coast. Estuar. Coast. Shelf Sci. 171, 35–40. https://doi.org/10.1016/j.ecss.2016.01.026.

Gaston, K.J., 2003. The Structure and Dynamics of Geographic Ranges. Oxford University Press, Oxford, UK.

Gaston, K.J., 2009. Geographic range limits of species: achieving synthesis. P. Roy. Soc. Lond. B. Bio. 276, 1395-1406. https://doi.org/10.1098/rspb.2008.1480.

Gómez-Gesteira, M., Decastro, M., Alvarez, I., Gesteira, J.L., 2008. Coastal Sea surface temperature warming trend along the continental part of the Atlantic Arc (1985–2005). J. Geophys. Res. 113. https://doi.org/10.1029/2007JC004315.

Grunnet, N.M., Walstra, D.-J.R., Ruessink, B.G., 2004. Process-based modelling of a shoreface nourishment. Coast. Eng. 51, 581–607. https://doi.org/10.1016/j.coastaleng.2004.07.016.

Helmuth, B., Mieszkowska, N., Moore, P., Hawkins, S.J., 2006. Living on the Edge of Two Changing Worlds: Forecasting the Responses of Rocky Intertidal Ecosystems to Climate Change. Annu. Rev. Ecol. Evol. Syst. 37, 373–404. https://doi.org/10.1146/annurev.ecolsys.37.091305.110149.

Iglesias, G., Carballo, R., Castro, A., 2008. Baroclinic modelling and analysis of tide- and wind-induced circulation in the Ría de Muros (NW Spain). J. Mar. Syst. 74, 475–484. https://doi.org/10.1016/j.jmarsys.2008.03.009.

Iglesias, G., Carballo, R., 2009. Seasonality of the circulation in the Ría de Muros (NW Spain). J. Mar. Syst. 78, 94–108. https://doi.org/10.1016/j.jmarsys.2009.04.002.

Iglesias, G., Carballo, R., 2010a. Wave energy and nearshore hot spots: The case of the SE Bay of Biscay. Renew. Energy 35, 2490–2500. https://doi.org/10.1016/j.renene.2010.03.016.

Iglesias, G., Carballo, R., 2010b. Effects of high winds on the circulation of the using a mixed open boundary condition: the Ría de Muros, Spain. Environ. Model. Softw. 25, 455–466. https://doi.org/10.1016/j.envsoft.2009.10.013.

IPCC, 2001. Climate change 2001: the scientific basis. In: Houghton, J.T., Ding, Y., Griggs, D.J., Noguer, M., van der Linden, P.J., Dai, X., Maskell, K., Johnson, C.A. (Eds.), Contribution of Working Group I to the Third Assessment Report of the Intergovernmental Panel on Climate Change. Cambridge University Press, Cambridge, United Kingdom and New York, NY, USA, p. 881.

IPCC, 2014: Climate Change 2014: Synthesis Report. Contribution of Working Groups I, II and III to the Fifth Assessment Report of the Intergovernmental Panel on Climate Change [Core Writing Team, R.K. Pachauri and L.A. Meyer (eds.)]. IPCC, Geneva, Switzerland, 151 pp.

IPCC, 2019: IPCC Special Report on the Ocean and Cryosphere in a Changing Climate [H.-O. Pörtner, D.C. Roberts, V. Masson-Delmotte, P. Zhai, M. Tignor, E. Poloczanska, K. Mintenbeck, A. Alegría, M. Nicolai, A. Okem, J. Petzold, B. Rama, N.M. Weyer (eds.)]. In press.

Jones, C.G., Lawron, J.H., Shachak, M., 1997. Positive and negative effects of organisms as physical ecosystem engineers. Ecology 78, 1946–1957. https://doi.org/10.1890/0012-9658(1997)078[1946:PANEOO]2.0.CO;2.

Jueterbock, A., Tyberghein, L., Verbruggen, H., Coyer, J.A., Olsen, J.L., Hoarau, G., 2013. Climate change impact on seaweed meadow distribution in the North Atlantic rocky intertidal. Ecol. Evol. 3, 1356–1373. https://doi.org/10.1002/ece3.541.

Keppel, G., Niel, K.P.V., Wardell-Johnson, G.W., Yates, C.J., Byrne, M., Mucina, L., Schut, A.G.T., Hopper, S.D., Franklin, S.E., 2012. Refugia: identifying and understanding safe havens for biodiversity under climate change. Glob. Ecol. Biogeogr. 21, 393–404. https://doi.org/10.1111/j.1466-8238.2011.00686.x.

Krumhansl, K.A., Okamoto, D.K., Rassweiler, A., Novak, M., Bolton, J.J., Cavanaugh, K.C., Connell, S.D., Johnson, C.R., Konar, B., Ling, S.D., Micheli, F., Norderhaug, K.M., Pérez-Matus, A., Sousa-Pinto, I., Reed, D.C., Salomon, A.K., Shears, N.T., Wernberg, T., Anderson, R.J., Barrett, N.S., Buschmann, A.H., Carr, M.H., Caselle, J.E., Derrien-Courtel, S., Edgar, G.J., Edwards, M., Estes, J.A., Goodwin, C., Kenner, M.C., Kushner, D.J., Moy, F.E., Nunn, J., Steneck, R.S., Vásquez, J., Watson, J., Witman, J.D., Byrnes, J.E.K., 2016. Global patterns of kelp forest change over the past half-century. Proc. Natl. Acad. Sci. U. S. A. 113, 13785–13790. https://doi.org/10.1073/pnas.1606102113.

Lesser, G.R., Roelvink, J.A., van Kester, J.A.T.M., Stelling, G.S., 2004. Development and validation of a three-dimensional morphological model. Coast. Eng., Coastal Morphodynamic Modeling 51, 883–915. https://doi.org/10.1016/j.coastaleng.2004.07.014.

Lima, F.P., Ribeiro, P.A., Queiroz, N., Hawkins, S.J., Santos, A.M., 2007. Do distributional shifts of northern and southern species of algae match the warming pattern? Glob. Change Biol. 13, 2592-2604. https://doi.org/10.1111/j.1365-2486.2007.01451.x.

Lourenço, C.R., Zardi, G.I., McQuaid, C.D., Serrão, E.A., Pearson, G.A., Jacinto, R., Nicastro, K.R., 2016. Upwelling areas as climate change refugia for the distribution and genetic diversity of a marine macroalga. J. Biogeogr. 43, 1595–1607. https://doi.org/10.1111/jbi.12744.

Luning, K., Yarish, C., Kirkman, H., 1990. Seaweeds: their environment, biogeography, and ecophysiology. Wiley.

MacMillan, D.S., Beckley, B.D., Fang, P., 2004. Monitoring the TOPEX and Jason-1 Microwave Radiometers with GPS and VLBI Wet Zenith Path Delays. Mar. Geod. 27, 703–716. https://doi.org/10.1080/01490410490904780.

Martínez, B., Viejo, R.M., Carreño, F., Aranda, S.C., 2012. Habitat distribution models for intertidal seaweeds: responses to climatic and non-climatic drivers. J. Biogeogr. 39, 1877–1890. https://doi.org/10.1111/j.1365-2699.2012.02741.x.

Martínez, B., Arenas, F., Trilla, A., Viejo, R.M., Carreño, F., 2015. Combining physiological threshold knowledge to species distribution models is key to improving forecasts of the future niche for macroalgae. Glob. Change Biol. 21, 1422–1433. https://doi.org/10.1111/gcb.12655.

Mendes, R., Vaz, N., Fernández-Nóvoa, D., da Silva, J.C.B., deCastro, M., Gómez-Gesteira, M., Dias, J.M., 2014. Observation of a turbid plume using MODIS imagery: The case of Douro estuary (Portugal). Remote Sens. Environ. 154, 127–138. https://doi.org/10.1016/j.rse.2014.08.003.

Merzouk, A., Johnson, L.E., 2011. Kelp distribution in the northwest Atlantic Ocean under a changing climate. J. Exp. Mar. Biol. Ecol., Global change in marine ecosystems 400, 90–98. https://doi.org/10.1016/j.jembe.2011.02.020.

Michel, S., Treguier, A.-M., Vandermeirsch, F., 2009. Temperature variability in the Bay of Biscay during the past 40 years, from an in situ analysis and a 3D global simulation. Cont. Shelf Res., 100 Years of Research within the Bay of Biscay 29, 1070–1087. https://doi.org/10.1016/j.csr.2008.11.019.

Nicastro, K.R., Zardi, G.I., Teixeira, S., Neiva, J., Serrão, E.A., Pearson, G.A., 2013. Shift happens: trailing edge contraction associated with recent warming trends threatens a distinct genetic lineage in the marine macroalga Fucus vesiculosus. BMC Biol. 11, 6. https://doi.org/10.1186/1741-7007-11-6.

Parmesan, C., Gaines, S., González, L., Kaufman, D.M., Kingsolver, J., Peterson, A.T., Sagarin, R., 2005. Empirical perspectives on species borders: from traditional biogeography to global change. Oikos 108, 58-75. https://doi.org/10.1111/j.0030-1299.2005.13150.x.

Pawlowicz, R., Beardsley, B., Lentz, S., 2002. Classical tidal harmonic analysis including error estimates in MATLAB using T_TIDE. Comput. Geosci. 28, 929–937. https://doi.org/10.1016/S0098-3004(02)00013-4.

Pecl, G.T., Araújo, M.B., Bell, J.D., Blanchard, J., Bonebrake, T.C., Chen, I.-C., Clark, T.D., Colwell, R.K., Danielsen, F., Evengård, B., Falconi, L., Ferrier, S., Frusher, S., Garcia, R.A., Griffis, R.B., Hobday, A.J., Janion-Scheepers, C., Jarzyna, M.A., Jennings, S., Lenoir, J., Linnetved, H.I., Martin, V.Y., McCormack, P.C., McDonald, J., Mitchell, N.J., Mustonen, T., Pandolfi, J.M., Pettorelli, N., Popova, E., Robinson, S.A., Scheffers, B.R., Shaw, J.D., Sorte, C.J.B., Strugnell, J.M., Sunday, J.M., Tuanmu, M.-N., Vergés, A., Villanueva, C., Wernberg, T., Wapstra, E., Williams, S.E., 2017. Biodiversity redistribution under climate change: Impacts on ecosystems and human well-being. Science 355. https://doi.org/10.1126/science.aai9214.

Pessarrodona, A., Foggo, A., Smale, D.A., 2019. Can ecosystem functioning be maintained despite climate-driven shifts in species composition? Insights from novel marine forests. J. Ecol. 107, 91–104. https://doi.org/10.1111/1365-2745.13053.

Prego, R., Bao, R., 1997. Upwelling influence on the Galician coast: silicate in shelf water and underlying surface sediments. Cont. Shelf Res. 17, 307–318. https://doi.org/10.1016/S0278-4343(96)00030-1.

Prego, R., Varela, M., 1998. Hydrography of the Artabro Gulf in summer: western coastal limit of Cantabrian seawater and wind-induced upwelling at prior cape. Oceanol. Acta, International Conference on Oceanography of the Bay of Biscay 21, 145–155. https://doi.org/10.1016/S0399-1784(98)80004-2.

Prego, R., Barciela, M. del C., Varela, M., 1999. Nutrient dynamics in the Galician coastal area (Northwestern Iberian Peninsula): Do the Rias Bajas receive more nutrient salts than the Rias Altas? Cont. Shelf Res. 19, 317–334. https://doi.org/10.1016/S0278-4343(98)00099-5.

Ramos, E., Guinda, X., Puente, A., de la Hoz, C.F., Juanes, J.A., 2020. Changes in the distribution of intertidal macroalgae along a longitudinal gradient in the northern coast of Spain. Mar. Environ. Res. 157, 104930. https://doi.org/10.1016/j.marenvres.2020.104930.

Rehm, E.M., Olivas, P., Stroud, J., Feeley, K.J., 2015. Losing your edge: climate change and the conservation value of range-edge populations. Ecol. Evol. 5, 4315–4326. https://doi.org/10.1002/ece3.1645.

Sagarin, R.D., Gaines, S.D., Gaylord, B., 2006. Moving beyond assumptions to understand abundance distributions across the ranges of species. Trends Ecol. Evol. 21, 524-530. https://doi.org/10.1016/j.tree.2006.06.008.

Santos, F., Gomez Gesteira, M., deCastro, M., 2011. Coastal and oceanic SST variability along the western Iberian Peninsula. Cont. Shelf Res. 31, 2012–2017. https://doi.org/10.1016/j.csr.2011.10.005.

Santos, F., deCastro, M., Gómez-Gesteira, M., Álvarez, I., 2012. Differences in coastal and oceanic SST warming rates along the Canary upwelling ecosystem from 1982 to 2010. Cont. Shelf Res. 47, 1–6. https://doi.org/10.1016/j.csr.2012.07.023.

Seabra, R., Varela, R., Santos, A.M., Gómez-Gesteira, M., Meneghesso, C., Wethey, D.S., Lima, F.P., 2019. Reduced Nearshore Warming Associated With Eastern Boundary Upwelling Systems. Front. Mar. Sci. 0. https://doi.org/10.3389/fmars.2019.00104.

Schiel, D.R., 2006. Rivets or bolts? When single species count in the function of temperate rocky reef communities. J. Exp. Mar. Biol. Ecol., Experimental marine ecology: a tribute to Professor Tony Underwood 338, 233–252. https://doi.org/10.1016/j.jembe.2006.06.023.

Smale, D.A., Burrows, M.T., Moore, P., O´Connor, N., Hawkins, S.J., 2013. Threats and knowledge gaps for ecosystem services provided by kelp forests: a northeast Atlantic perspective - Smale - 2013 - Ecology and Evolution - Wiley Online Library. Ecol Evol 3, 4016–4038. https://doi.org/10.1002/ece3.774.

Smale, D.A., Wernberg, T., 2013. Extreme climatic event drives range contraction of a habitat-forming species. Proc. R. Soc. B Biol. Sci. 280, 20122829. https://doi.org/10.1098/rspb.2012.2829.

Sousa, M.C., Vaz, N., Alvarez, I., Gomez-Gesteira, M., Dias, J.M., 2014a. Modeling the Minho River plume intrusion into the Rias Baixas (NW Iberian Peninsula). Cont. Shelf Res. 85, 30–41. https://doi.org/10.1016/j.csr.2014.06.004.

Sousa, M.C., Vaz, N., Alvarez, I., Gomez-Gesteira, M., Dias, J.M., 2014b. Influence of the Minho River plume on the Rias Baixas (NW of the Iberian Peninsula). J. Mar. Syst. 139, 248–260. https://doi.org/10.1016/j.jmarsys.2014.06.012.

Sousa, M.C., deCastro, M., Alvarez, I., Gomez-Gesteira, M., Dias, J.M., 2017. Why coastal upwelling is expected to increase along the western Iberian Peninsula over the next century? Sci. Total Environ. 592, 243–251. https://doi.org/10.1016/j.scitotenv.2017.03.046.

Sousa, M.C., Ribeiro, A.S., Des, M., Mendes, R., Alvarez, I., Gomez Gesteira, M., Dias, J.M., 2018. Integrated High-resolution Numerical Model for the NW Iberian Peninsula Coast and Main Estuarine Systems. J Coast Res 85, 66–70. https://doi.org/10.2112/SI85-014.1.

Sousa, M.C., Ribeiro, A., Des, M., Gomez-Gesteira, M., deCastro, M., Dias, J.M., 2020. NW Iberian Peninsula coastal upwelling future weakening: Competition between wind intensification and surface heating. Sci. Total Environ. 703, 134808. https://doi.org/10.1016/j.scitotenv.2019.134808.

Steneck, R.S., Graham, M.H., Bourque, B.J., Corbett, D., Erlandson, J.M., Estes, J.A., Tegner, M.J., 2002.

Kelp forest ecosystems: biodiversity, stability, resilience and future. Environ. Conserv. 29, 436–459. https://doi.org/10.1017/S0376892902000322.

Sutherland, J., Walstra, D.J.R., Chesher, T.J., van Rijn, L.C., Southgate, H.N., 2004. Evaluation of coastal area modelling systems at an estuary mouth. Coast. Eng. 51, 119–142. https://doi.org/10.1016/j.coastaleng.2003.12.003.

Sydeman, W.J., García-Reyes, M., Schoeman, D.S., Rykaczewski, R.R., Thompson, S.A., Black, B.A., Bograd, S.J., 2014. Climate change and wind intensification in coastal upwelling ecosystems. Science 345, 77–80. https://doi.org/10.1126/science.1251635.

Teagle, H., Hawkins, S.J., Moore, P.J., Smale, D.A., 2017. The role of kelp species as biogenic habitat formers in coastal marine ecosystems. J. Exp. Mar. Biol. Ecol., Ecological responses to environmental change in marine systems 492, 81–98. https://doi.org/10.1016/j.jembe.2017.01.017.

Thomas, C.D., Franco, A.M.A., Hill, J.K., 2006. Range retractions and extinction in the face of climate warming. Trends Ecol. Evol. 21, 415-416. https://doi.org/10.1016/j.tree.2006.05.012.

Varela, R., Álvarez, I., Santos, F., deCastro, M., Gómez-Gesteira, M., 2015. Has upwelling strengthened along worldwide coasts over 1982-2010? Sci. Rep. 5, 10016. https://doi.org/10.1038/srep10016.

Varela, R., Lima, F.P., Seabra, R., Meneghesso, C., Gómez-Gesteira, M., 2018. Coastal warming and wind-driven upwelling: A global analysis. Sci. Total Environ. 639, 1501–1511. https://doi.org/10.1016/j.scitotenv.2018.05.273.

Walther, G.R., Post, E., Convey, P., Menzel, A., Parmesan, C., Beebee, T.J.C., Fromentin, J-M., Hoegh-Guldberg O., Bairlein, F., 2002. Ecological responses to recent climate change. Nature 416, 389–395. https://doi.org/10.1038/416389a..

Wang, D., Gouhier, T.C., Menge, B.A., Ganguly, A.R., 2015. Intensification and spatial homogenization of coastal upwelling under climate change. Nature 518, 390–394. https://doi.org/10.1038/nature14235.

Warner, J.C., Geyer, W.R., Lerczak, J.A., 2005. Numerical modeling of an estuary: A comprehensive skill assessment. J. Geophys. Res. 110. https://doi.org/10.1029/2004JC002691.

Wernberg, T., Smale, D., Tuya, F., Thomsen, M., Langlois, T., Bettignies, T.D., Bennett, S., Rousseaux, C.S., 2013. An extreme climatic event alters marine ecosystem structure in a global biodiversity hotspot. Nat. Clim. Change 2012/7. https://doi.org/10.1038/NCLIMATE1627.

Wernberg, T., Bennett, S., Babcock, R.C., de Bettignies, T., Cure, K., Depczynski, M., Dufois, F., Fromont, J., Fulton, C.J., Hovey, R.K., Harvey, E.S., Holmes, T.H., Kendrick, G.A., Radford, B., Santana-Garcon, J., Saunders, B.J., Smale, D.A., Thomsen, M.S., Tuckett, C.A., Tuya, F., Vanderklift, M.A., Wilson, S., 2016. Climate-driven regime shift of a temperate marine ecosystem. Science 353, 169–172. https://doi.org/10.1126/science.aad8745.

Wernberg, T., Krumhansl, K., Filbee-Dexter, K., Pedersen, M.F., 2019. Chapter 3 - Status and Trends for the World's Kelp Forests, in: Sheppard, C. (Ed.), World Seas: An Environmental Evaluation (Second Edition). Academic Press, pp. 57–78. https://doi.org/10.1016/B978-0-12-805052-1.00003-6.

Wiens, J.J., 2016. Climate-Related Local Extinctions Are Already Widespread among Plant and Animal Species. PLOS Biol. 14, e2001104. https://doi.org/10.1371/journal.pbio.2001104.

Wilson, K.L., Skinner, M.A., Lotze, H.K., 2019. Projected 21st-century distribution of canopy-forming seaweeds in the Northwest Atlantic with climate change. Divers. Distrib. 25, 582–602. https://doi.org/10.1111/ddi.12897.